BELLE2-NOTE-PH-2018-004
DRAFT Version 1.0
June 29, 2018

Rediscovery of $D^{*(0)}$ and B in Belle II with phase II data

V. Bhardwaj*

Indian Institute of Science Education and Research (IISER), Mohali, India

K. Trabelsi†

High Energy Accelerator Research Organization (KEK), Tsukuba, Japan

N. Rout‡ and Resmi. P.K.§

Indian Institute of Technology Madras, India

S. Maity¶

Indian Institute of Technology Bhubaneswar, India

E. Ganiev** and D. Tonelli††

INFN, Trieste

Abstract

This note describes rediscovery of $D^{(*)}$, $D^{(*0)}$ and B modes in Experiment3 data.

*Electronic address: vishal@iisermohali.ac.in
†Electronic address: karim.trabelsi@kek.jp
‡Electronic address: niharikarout@physics.iitm.ac.in
§Electronic address: resmipk@physics.iitm.ac.in
¶Electronic address: sm46@iitbbs.ac.in
**Electronic address: Eldar.Ganiev@ts.infn.it
††Electronic address: diego.tonelli@cern.ch

Contents

1. INTRODUCTION

This note describes $D^{(*)}$ reconstruction on analysis level in early Exp3 data and provides information required to obtain those plots. Then detailed analysis of D^* with a variety of D final states is performed in data and MC. In the end, B meson reconstruction to $D^{(*)}h$ final sate is also discussed. In Section 2, a brief description of the dataset used is given, selection is described in Section 3. The $D^{*\pm}$ rediscoveries are discussed in Section 4, 5 and 6. Section 7 describes the rediscoveries of D^{*0} meson. B meson rediscoveries are given in Section 9.

2. DATASETS

All plots in this note are based on the reprocessed data from Experiment 3. The data is skimmed based on the 'hlt_hadron' skim flag. These

skimmed files are provided at /ghi/fs01/belle2/bdata/users/karim/skims/release-01-02-03/DB00000382/prod00000002/e0003/. The data is reconstructed using release-01-02-03 and the global tag GT382 (GT_gen_data_004.51_reprocessing-release-01-02-03) including the magnetic field MagneticFieldPhase2-2018-04 for prod2. Reconstruction is done with release-01-02-07 for prod3. Dress rehearsal 2 (DR2) samples located at /ghi/fs01/belle2/bdata/users/karim/MC/DR2/release-01-00-01/mdst/ (1 fb^{-1})are used for MC studies. These sample are created to check the data flow of Belle II, but serve as a good sample to test data-MC agreement. They contain $q\bar{q}$, $\mu\mu$, $\tau\tau$ processes.

3. SELECTION

The 'hlt_hadron' HLT skim selects events with at least three tracks from the IP region (nTracksLE >= 3) that is not a Bhabha event (Bhabha2Trk==0).

The selection is the one used in the monitoring package of the data production group where the PID cuts have been removed. D candidates are reconstructed from the corresponding final states. Charged tracks are selected with impact parameters d_0 and z_0 with an absolute values respectively less than 0.5 and 3 cm. A pion is added to the D candidate to form a D^* candidate and the momentum in center-of-mass of this candidate is requested to be more than 2.5 GeV/c to select cleaner D^* from $c\bar{c}$ events. The following criteria are applied:

- $1.7 < M_D < 2.1$ GeV/c^2
- $0.14 < \Delta M < 0.16$ GeV/c^2, where ΔM is defined as $M(D^*) - M(D)$

PID cuts have been checked in prod3 sample.

4. $D^{*\pm}$ MODES IN PROD2

In this section we look at $D^{*\pm}$ modes $D \to K\pi, K\pi\pi^0$ and $K\pi\pi\pi$ in prod2 data. These are Cabibbo favoured (CF) final states.

4.1. $D^{*\pm} \to D(K^-\pi^+)\pi^\pm$

Fig. 1 shows the 2D plot of ΔM and $M(K\pi)$ as well as the signal-enhanced plots in the early data of integrated luminosity 5 pb^{-1} (runs 112-1355).

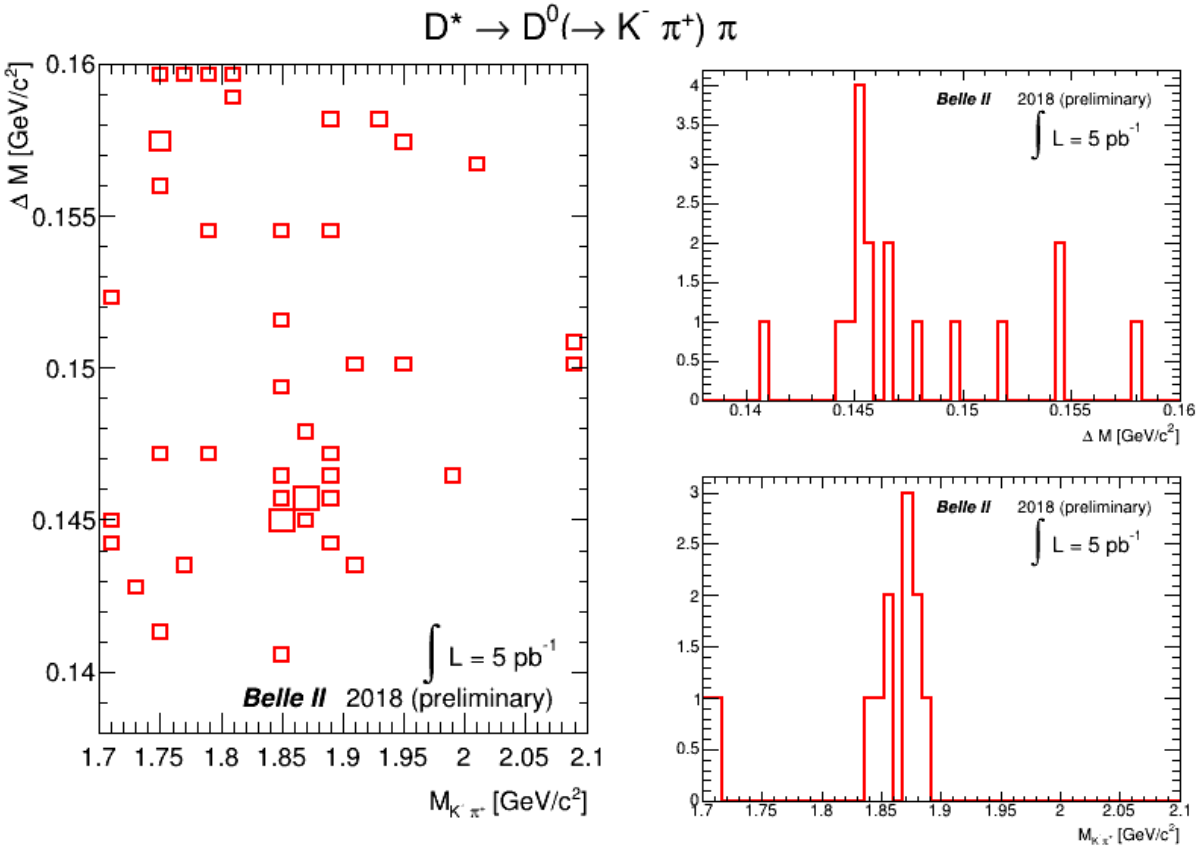

FIG. 1: 2D plot of ΔM and $M(K\pi)$ (left), signal-enhanced plots: ΔM for $1.845 < M(K\pi) < 1.885$ GeV/c^2 (right top) and $M(K\pi)$ for $0.144 < \Delta M < 0.146$ GeV/c^2 (right bottom)

The mode was studied in DR2 sample. A two dimensional maximum likelihood fit is performed between ΔM and M_D. There are three components: signal, combinatorial background and events with correct D but fake D^* due to the presence of a random π. The signal components are modelled with Gaussian function for both ΔM and M_D. The combinatorial background is modelled with a threshold function $((\Delta M - m_\pi)^\alpha \exp(-\beta(\Delta M - m_\pi)))$ for ΔM and first order polynomial for M_D. The random slow π component has signal shape itself for M_D and threshold function for ΔM. The fit projections are shown in Fig. 2. The signal region is defined as $1.845 < M_D < 1.885$ GeV/c^2 and $0.144 < \Delta M < 0.146$ GeV/c^2.

Fig. 3 shows the 2D plot of ΔM and M_D as well as the signal-enhanced plots in prod2 data (runs 112-2531) corresponding to an integrated luminosity of 92 pb^{-1}. D daughter particles are kinematically constrained to nominal D mass.

Two dimensional fit in data sample is performed in data with fixing all the shape parameters from DR2 fit. Mean, fudge factors on σ and yields are only floated. The projections are shown in Fig. 4.

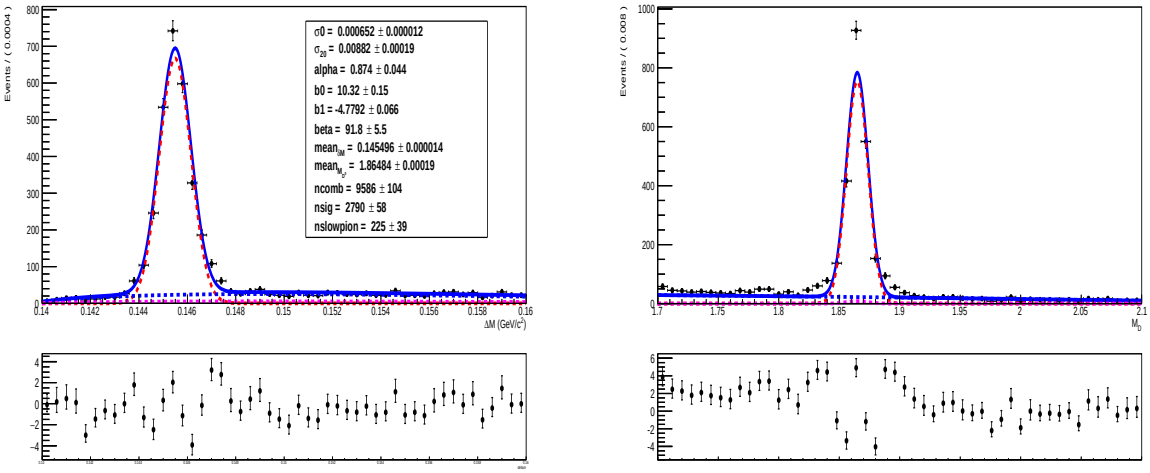

FIG. 2: ΔM (left) and M_D (right) signal-enhanced projections in DR2 sample for $D \to K\pi$ final state

4.2. $D^{*\pm} \to D(K^-\pi^+\pi^0)\pi^\pm$

Here, π^0 is selected from `veryLooseFit` list. Fig. 5 shows the 2D plot of ΔM and M_D as well as the signal-enhanced plots in 92 pb^{-1} prod2 data.

4.3. $D^{*\pm} \to D(K^-\pi^+\pi^-\pi^+)\pi^\pm$

The fit projections of a two dimensional maximum likelihood fit in DR2 sample are shown in Fig. 6. The 2D plot of ΔM and M_D as well as the signal-enhanced plots in 92 pb^{-1} prod2 data are shown in Fig. 7. The fit in prod2 data sample is shown in Fig. 8.

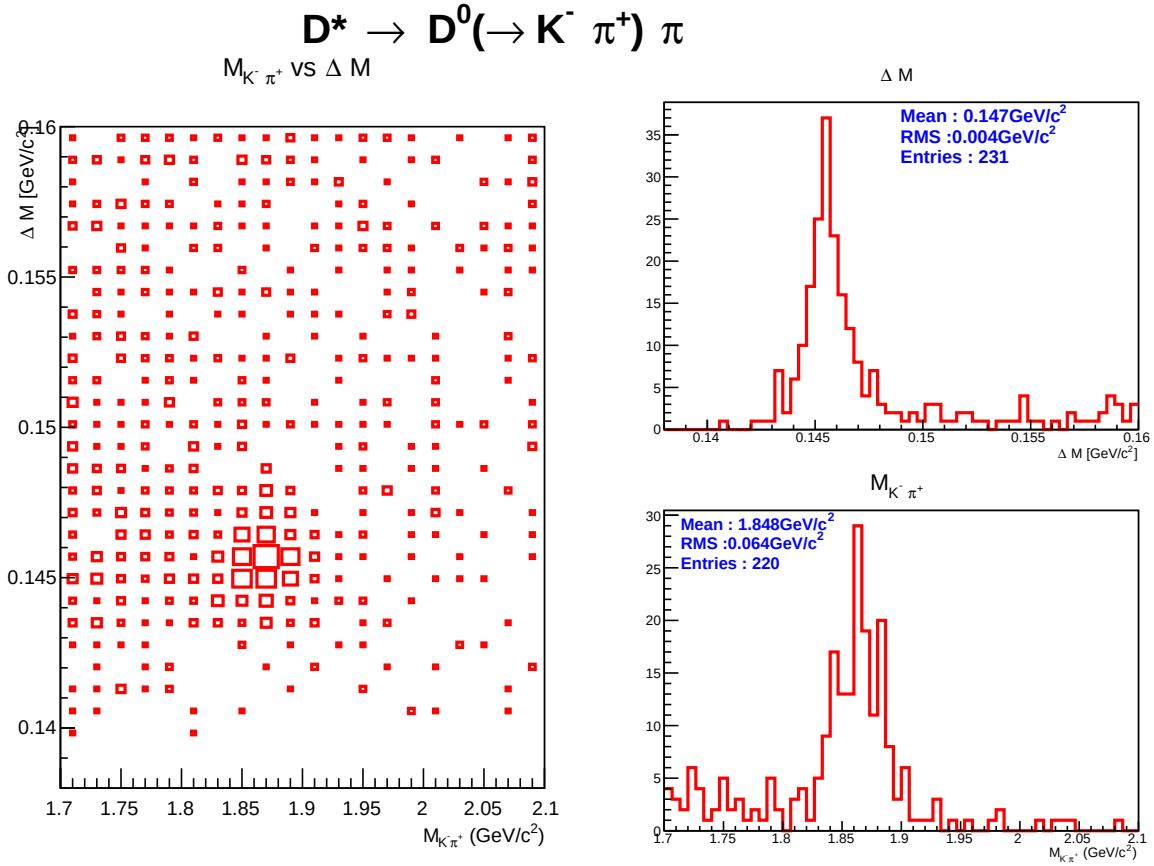

FIG. 3: 2D plot of ΔM and M_D (left), signal-enhanced plots: ΔM (right top) and M_D (right bottom) for $D \to K\pi$ final state

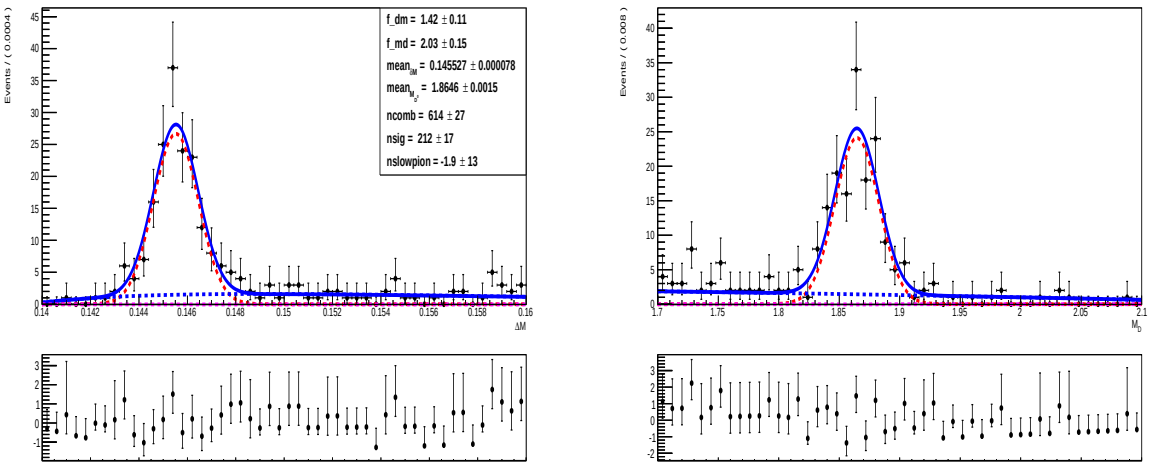

FIG. 4: ΔM (left) and M_D (right) signal-enhanced projections in prod2 data sample for $D \to K\pi$ final state

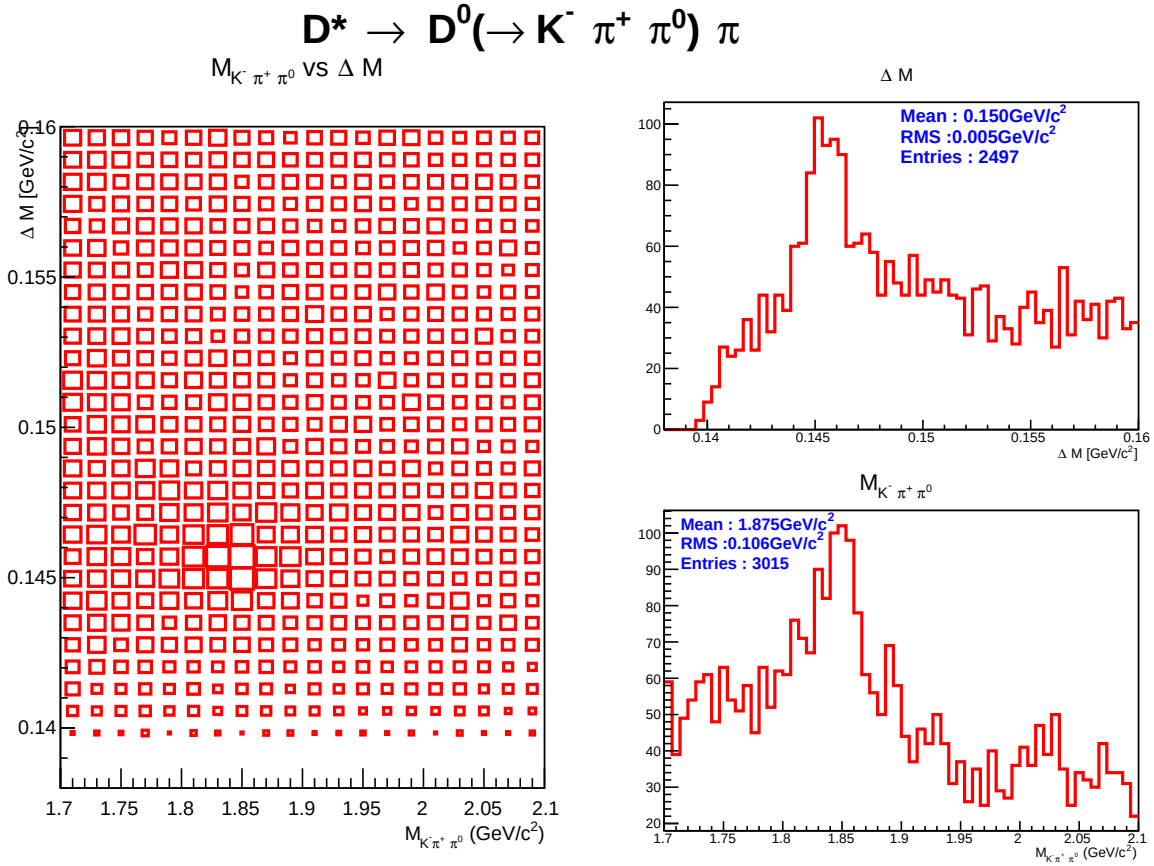

FIG. 5: 2D plot of ΔM and M_D (left), signal-enhanced plots: ΔM (right top) and M_D (right bottom) for $D \to K\pi\pi^0$ final state.

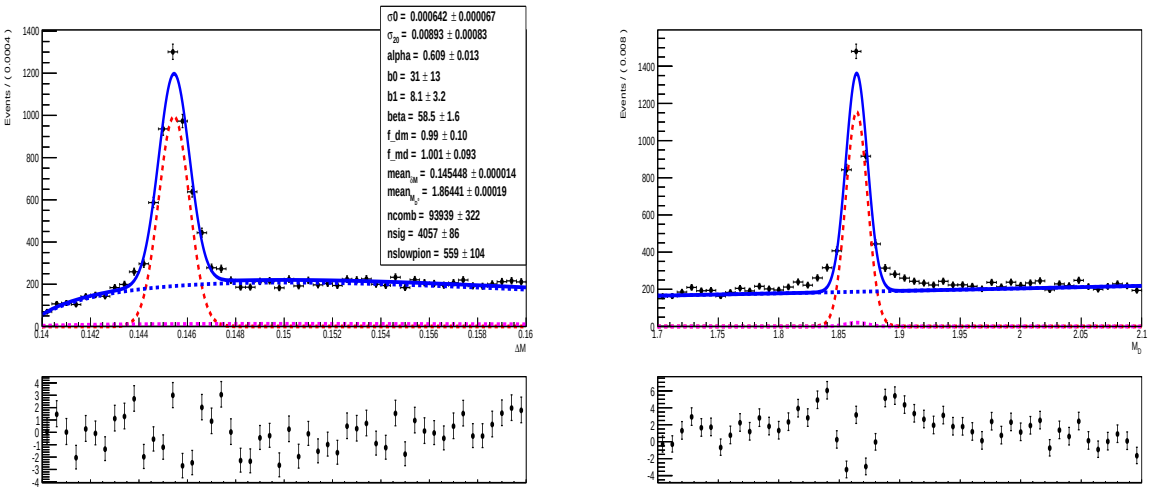

FIG. 6: ΔM (left) and M_D (right) signal-enhanced projections in DR2 sample for $D \to K\pi\pi\pi$ final state

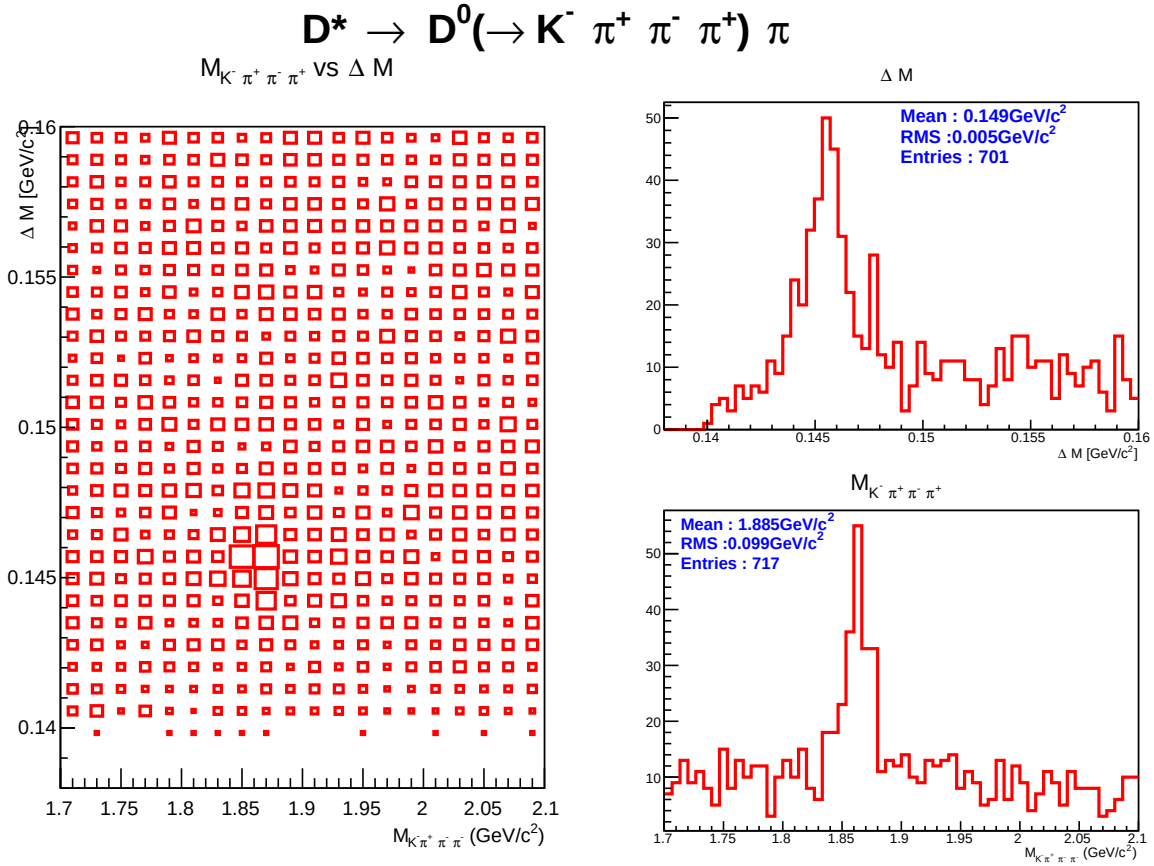

FIG. 7: 2D plot of ΔM and $M(K\pi\pi\pi)$ (left), signal-enhanced plots: ΔM (right top) and M_D (right bottom)

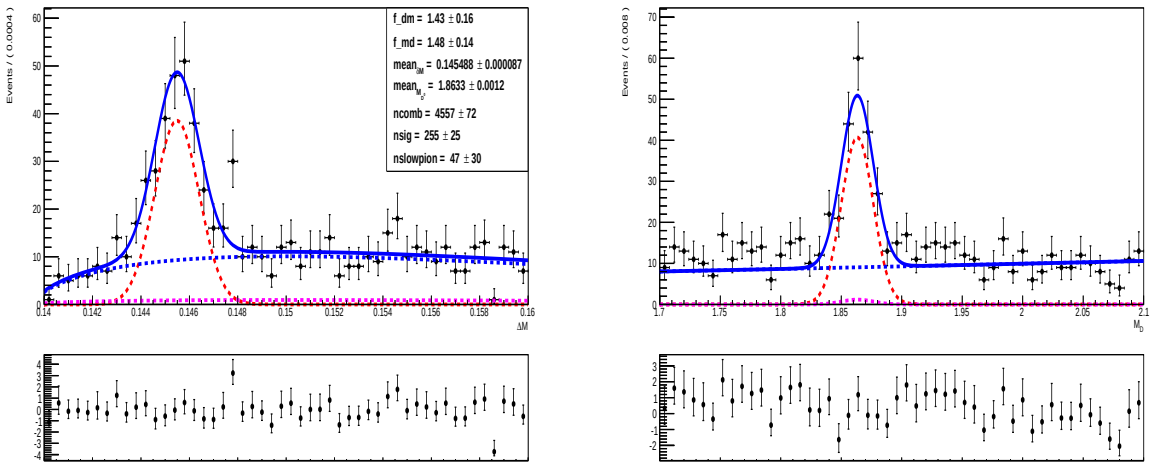

FIG. 8: ΔM (left) and M_D (right) signal-enhanced projections in prod2 data sample for $D \to K\pi\pi\pi$ final state.

A comparison of prod2 data and DR2 is shown in table I.

	DR2 1 fb^{-1}	data
Luminosity	1 fb^{-1}	92 pb^{-1} (prod2)
$K\pi$		
Nsig	2790±58	212±17
Ncomb	9586±104	614±27
Nrsp	225±39	-1.9±13
mean$_{\Delta M}$	0.145496±0.000014	0.145527±0.000078
$\sigma_{\Delta M}/f_{\Delta M}$	0.000652±0.000012	1.42±0.11
mean$_{M_D}$	1.86484±0.00019	1.8646±0.0015
σ_{M_D}/f_{M_D}	0.00882±0.00019	2.03±0.15
$K\pi\pi\pi$		
Nsig	4057±86	255±25
Ncomb	93939±322	4557±72
Nrsp	559±104	47±30
mean$_{\Delta M}$	0.145448±0.000014	0.145488±0.000087
$\sigma_{\Delta M}/f_{\Delta M}$	0.000642±0.000067	1.43±0.16
mean$_{M_D}$	1.86441±0.00019	1.8633±0.0012
σ_{M_D}/f_{M_D}	0.00893±0.00083	1.48±0.14

TABLE I: The fit parameter comparison between DR2 and prod2 data.

The resolution is 1.5 to 2 times worse in data than MC.

5. $D^{*\pm}$ MODES IN PROD3

In prod3, some of the bad runs have been removed. The runs where CDC, ECL or TOP absent have also been removed. The detector constants have been improved. New globaltag:GT399 was introduced with updated software. The total integrated luminosity is 88 pb^{-1} with runs 529-2531.

The ΔM and M_D distributions for $D \to K\pi$, $D \to K\pi\pi^0$ and $D \to K\pi\pi\pi$ final state are shown in Fig. 9, 10, 11.

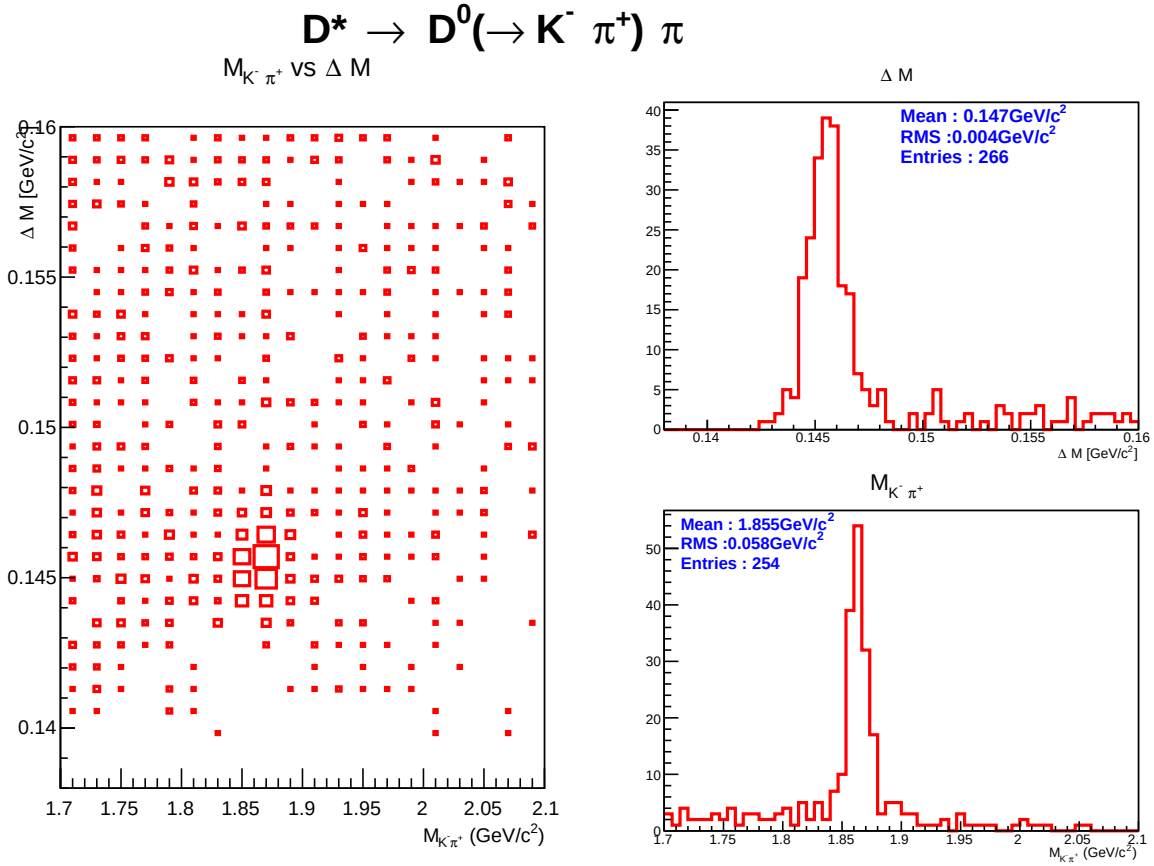

FIG. 9: 2D plot of ΔM and M_D (left), signal-enhanced plots: ΔM (right top) and M_D (right bottom) for $D \to K\pi$ final state.

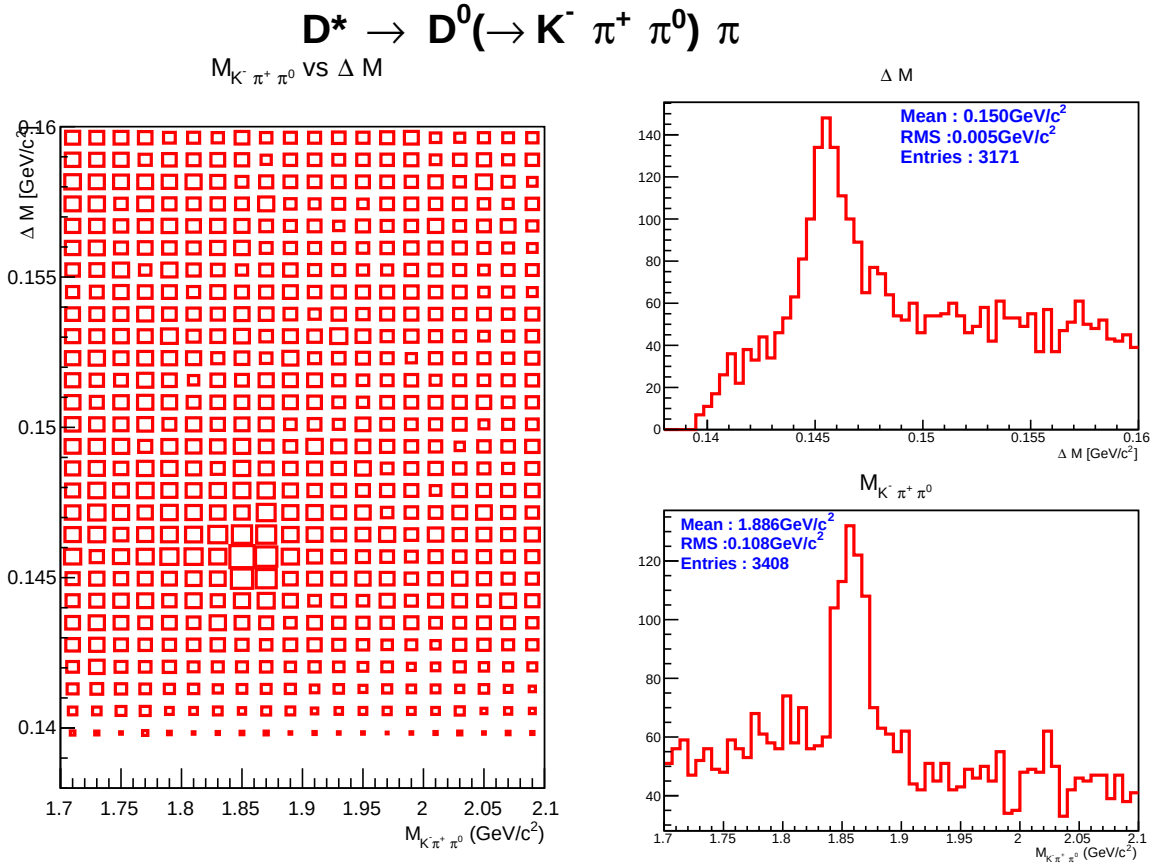

FIG. 10: 2D plot of ΔM and M_D (left), signal-enhanced plots: ΔM (right top) and M_D (right bottom) for $D \to K\pi\pi^0$ final state.

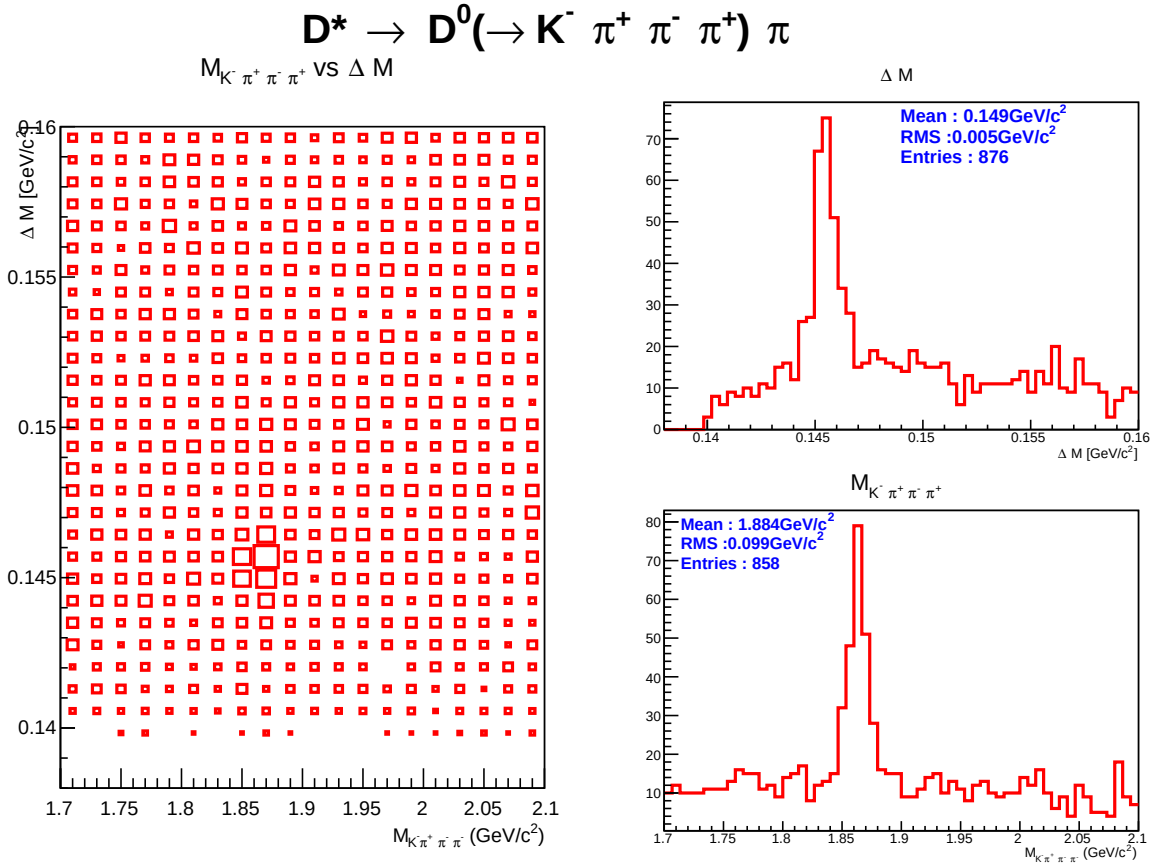

FIG. 11: 2D plot of ΔM and M_D (left), signal-enhanced plots: ΔM (right top) and M_D (right bottom) for $D \to K\pi\pi\pi$ final state.

The fit projections in prod3 data are shown in Fig. 12, 13.

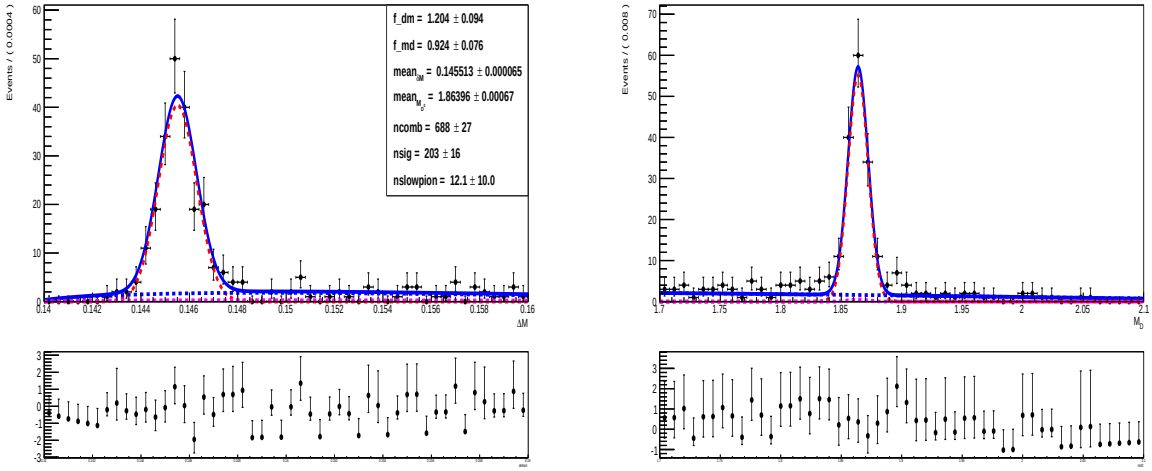

FIG. 12: ΔM (left) and $M(_D$ (right) signal-enhanced projections in prod3 data sample for $D \to K\pi$ final state.

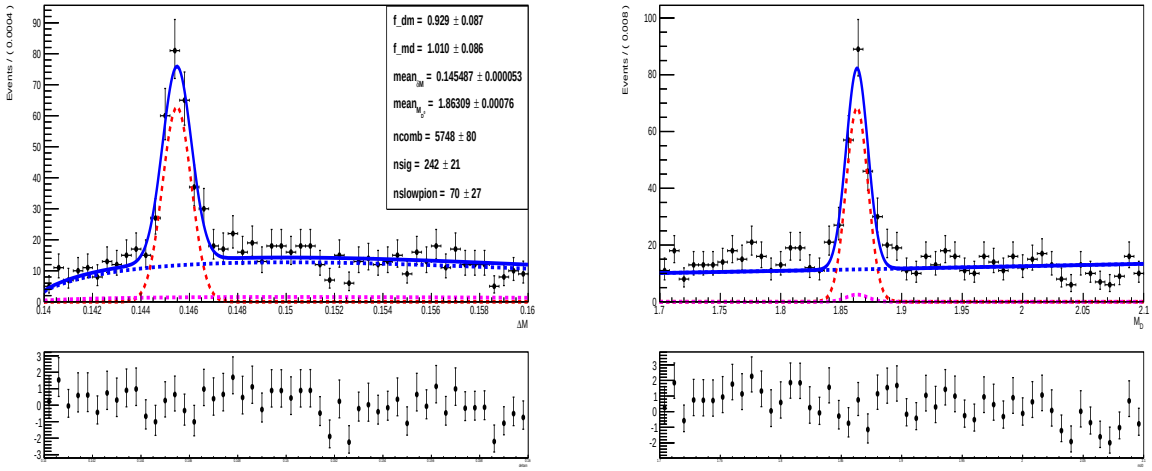

FIG. 13: ΔM (left) and $M(_D$ (right) signal-enhanced projections in prod3 data sample for $D \to K\pi\pi\pi$ final state.

The performance comparison between DR2, prod2 data and prod3 data are summarized in table II. Resolution is significantly improved in prod3 data.

	DR2 1 fb^{-1}	data prod2	data prod3
Luminosity	1 fb^{-1}	92 pb^{-1}	84 pb^{-1}
$K\pi$			
mean$_{\Delta M}$	0.145496±0.000014	0.145527±0.000078	0.145513±0.000065
$\sigma_{\Delta M}/f_{\Delta M}$	0.000652±0.000012	**1.42±0.11**	**1.204±0.094**
mean$_{M_D}$	1.86484±0.00019	1.8646±0.0015	1.86396±0.00067
σ_{M_D}/f_{M_D}	0.00882±0.00019	**2.03±0.15**	**0.924±0.076**
$K\pi\pi\pi$			
mean$_{\Delta M}$	0.145448±0.000014	0.145488±0.000087	0.145487±0.000053
$\sigma_{\Delta M}/f_{\Delta M}$	0.000642±0.000067	**1.43±0.16**	**0.929±0.087**
mean$_{M_D}$	1.86441±0.00019	1.8633±0.0012	1.86309±0.00076
σ_{M_D}/f_{M_D}	0.00893±0.00083	**1.48±0.14**	**1.010±0.086**

TABLE II: Fit parameter comparison between DR2, prod2 data and prod3 data.

5.1. PID performance

PID cut of > 0.5 is applied to K in all the three modes and the distributions are shown in Fig. 14, 15, 16. There is clear reduction in background with the application of PID cut.

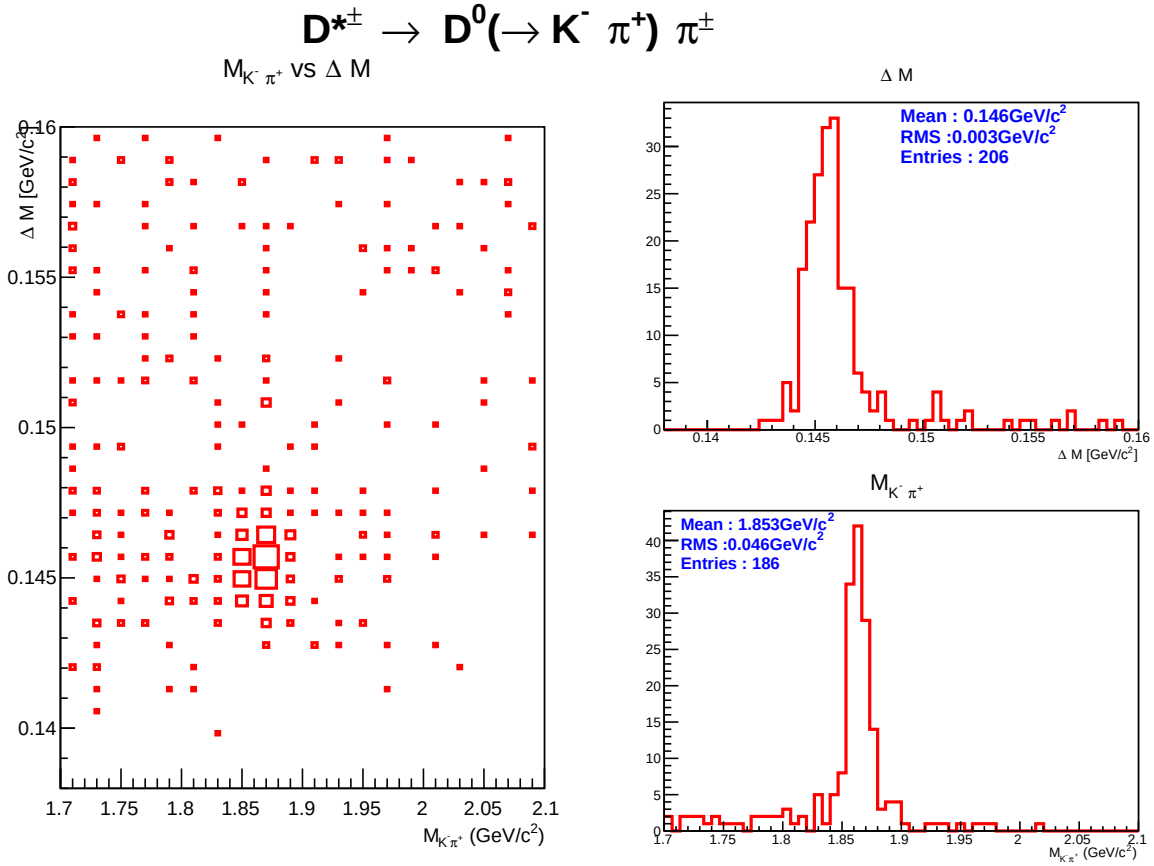

FIG. 14: 2D plot of ΔM and M_D (left), signal-enhanced plots: ΔM (right top) and M_D (right bottom) for $D \to K\pi$ final state with PID > 0.5 for K in prod3 data.

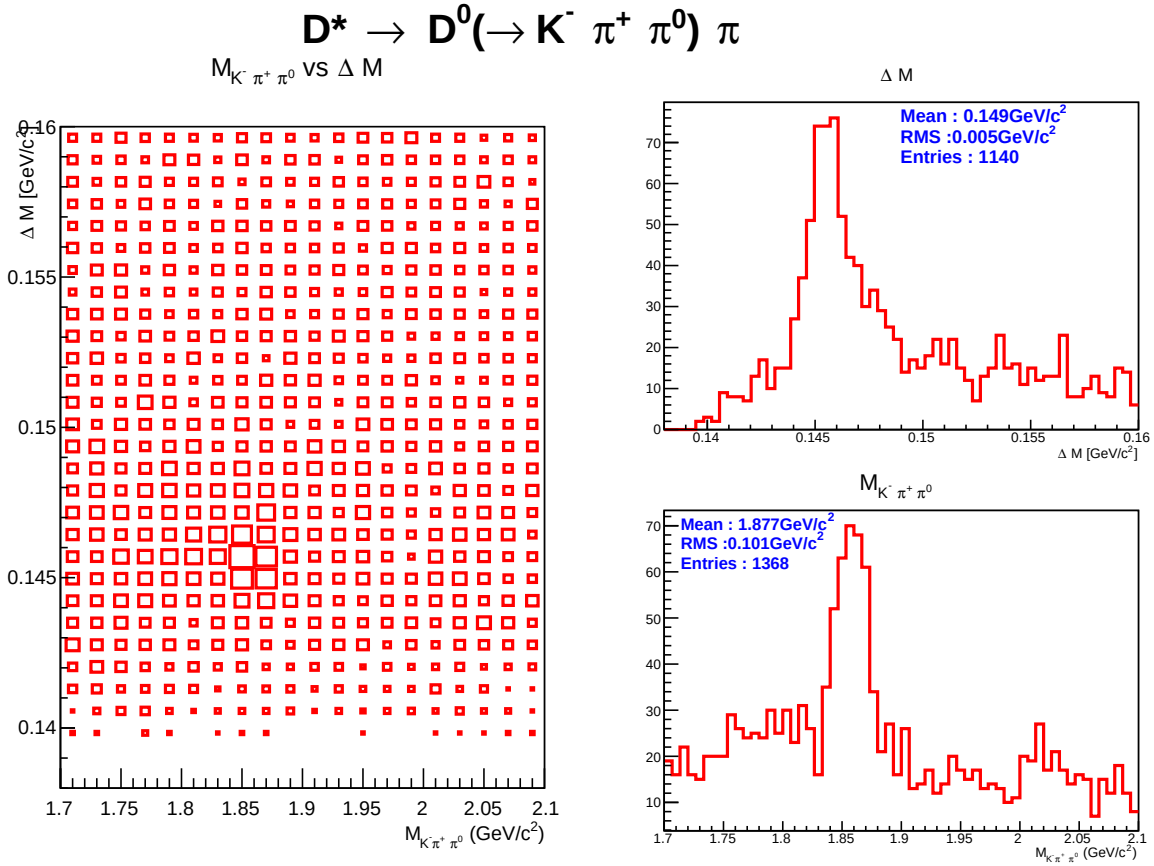

FIG. 15: 2D plot of ΔM and M_D (left), signal-enhanced plots: ΔM (right top) and M_D (right bottom) for $D \to K\pi\pi^0$ final state with PID > 0.5 for K in prod3 data.

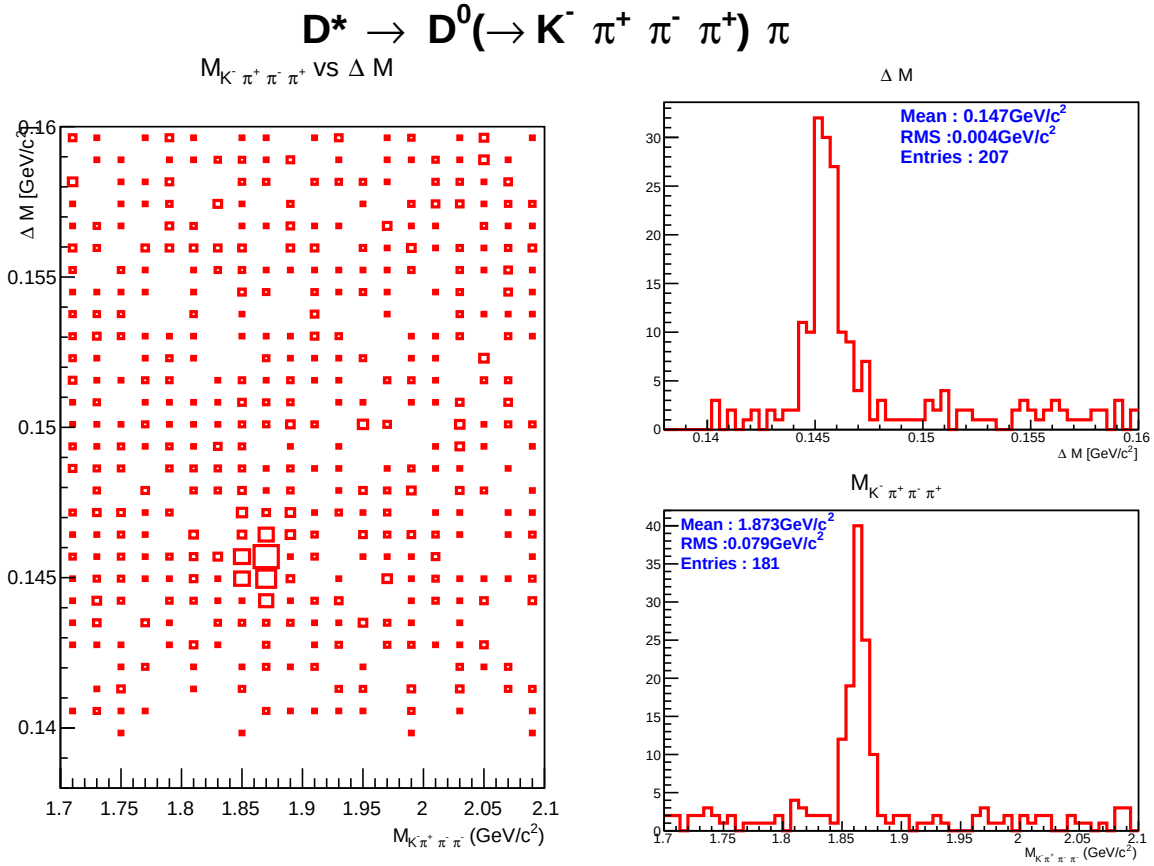

FIG. 16: 2D plot of ΔM and M_D (left), signal-enhanced plots: ΔM (right top) and M_D (right bottom) for $D \to K\pi\pi\pi$ final state with PID > 0.5 for K in prod3 data.

5.2. 250 pb^{-1} prod3 data

All the CF final states have been studied in 250 pb^{-1} prod3 data. PID cut > 0.5 is applied on K. The ΔM and M_D distributions are shown in Fig. 17, 18, 19.

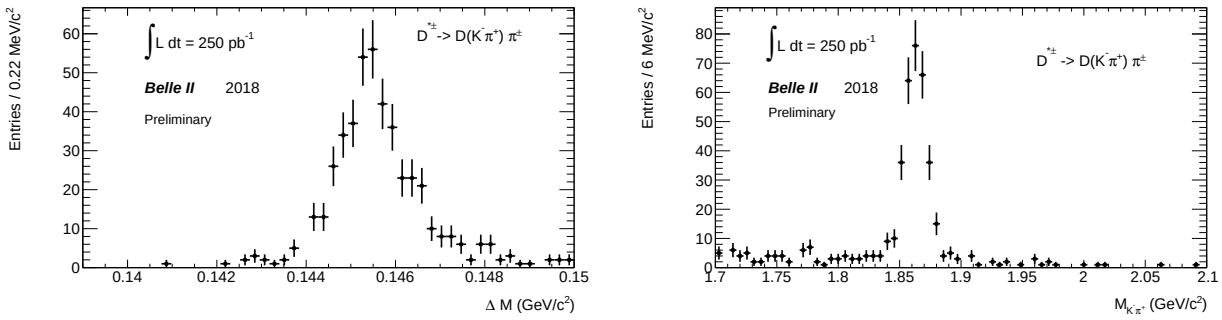

FIG. 17: ΔM (left) and M_D (right) signal-enhanced projections in 250 pb^{-1} prod3 data sample for $D \to K\pi$ final state.

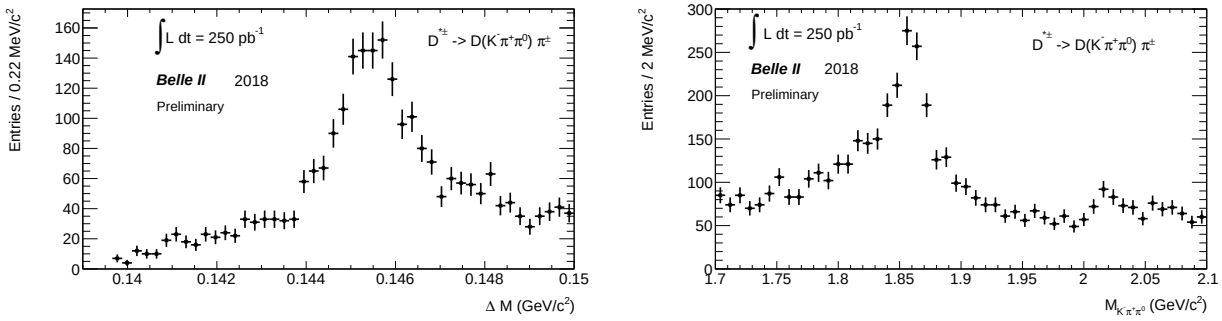

FIG. 18: ΔM (left) and M_D (right) signal-enhanced projections in 250 pb^{-1} prod3 data sample for $D \to K\pi\pi^0$ final state.

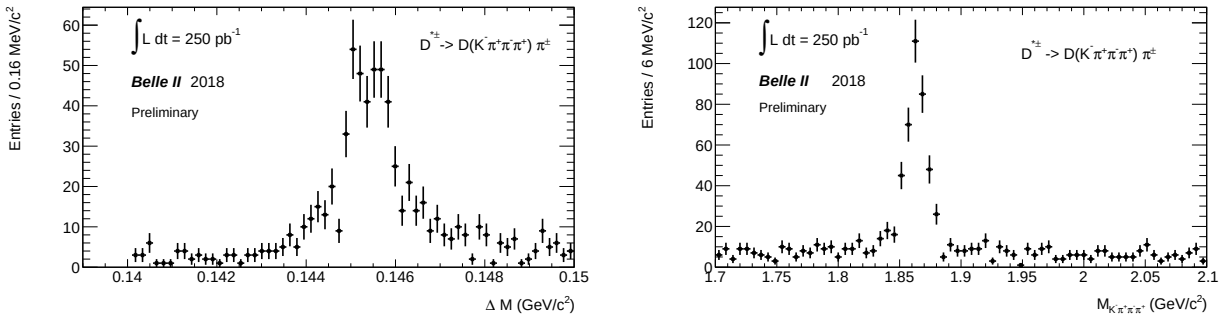

FIG. 19: ΔM (left) and M_D (right) signal-enhanced projections in 250 pb^{-1} prod3 data sample for $D \to K\pi\pi\pi$ final state.

5.3. 250 pb^{-1} prod4 data

In prod4, the detector constants have been further improved and PID performance is also improved. The CF final states are analysed and the ΔM and M_D distributions are shown in Fig. 20, 21, 22.

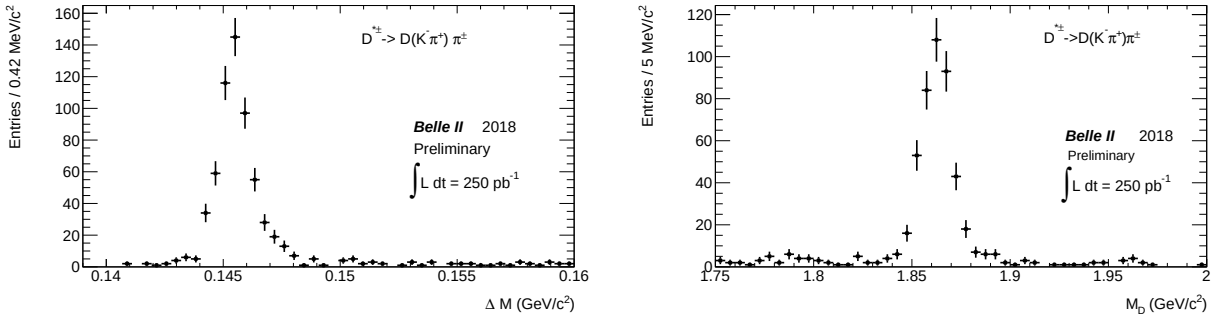

FIG. 20: ΔM (left) and M_D (right) signal-enhanced projections in 250 pb^{-1} prod4 data sample for $D \to K\pi$ final state.

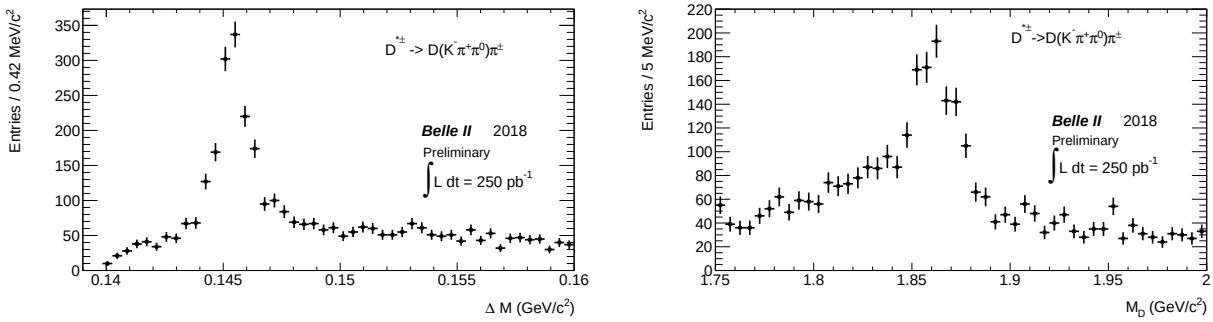

FIG. 21: ΔM (left) and M_D (right) signal-enhanced projections in 250 pb^{-1} prod4 data sample for $D \to K\pi\pi^0$ final state.

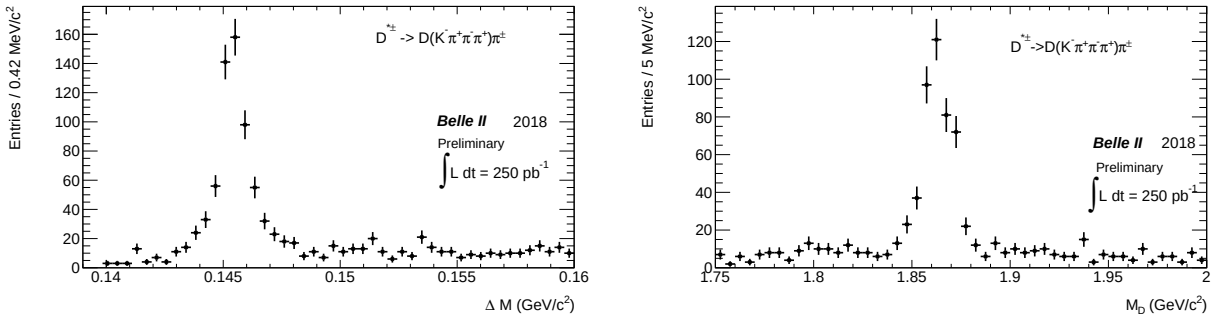

FIG. 22: ΔM (left) and M_D (right) signal-enhanced projections in 250 pb^{-1} prod4 data sample for $D \to K\pi\pi\pi$ final state.

5.3.1. *PID performances in prod4*

As we expect PID improvement in prod4, the yields are compared with and without PID for $K\pi$ and $K\pi\pi\pi$ modes. First a 2D fit is performed in DR2 sample for both the cases. In prod4 data sample, the shape parameters are fixed from DR2 sample except mean and fudge factor on σ.

Here, the signal component is modelled with Double Gaussian. For combinatorial, we have used the same model as described in Section 4.

Fig. 23, Fig. 24 shows 2D fit projections in DR2 sample and Fig. 25, Fig. 26 in prod4 data without PID.

Fig. 27, Fig. 28 shows 2D fit projections in DR2 sample and Fig. 29, Fig. 30 in prod4 data with PID.

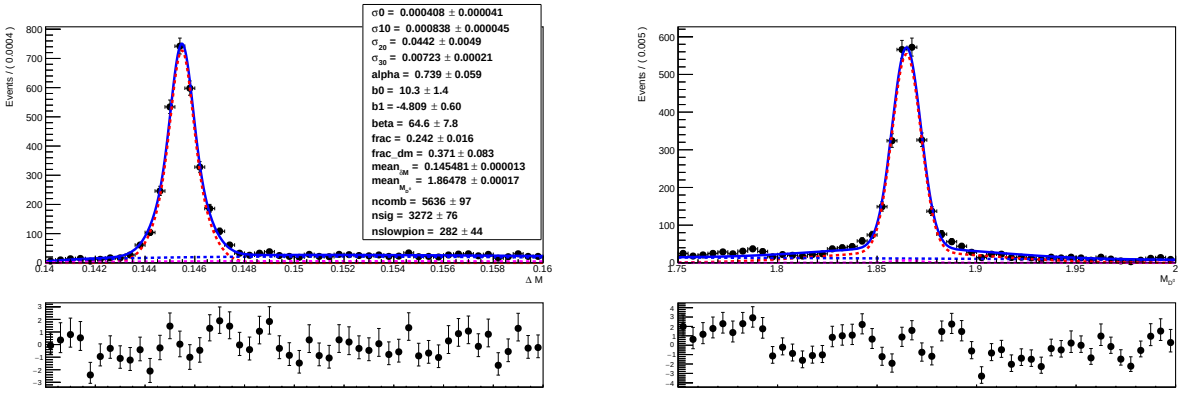

FIG. 23: ΔM (left) and M_D (right) 2D fit projections in DR2 sample for $D \to K\pi$ final state without PID.

Table IV summarizes the yields with and without PID in both DR2 and prod4 data sample.

Mode	yield			
	Without PID		With PID	
	DR2	Data	DR2	Data
$D \to K^-\pi^+$	3272 ± 76	749 ± 31	2870 ± 66	626 ± 27
$D \to K^-\pi^+\pi^-\pi^+$	5690 ± 150	839 ± 46	3769 ± 78	567 ± 29

TABLE III: Yields of $D^{*\pm}$ modes in 1 fb^{-1} DR2 and 250 pb^{-1} prod4 data sample. The yields are estimated from a two dimensional fit between M_D and ΔM. PID > 0.5 is applied for K in with PID cases.

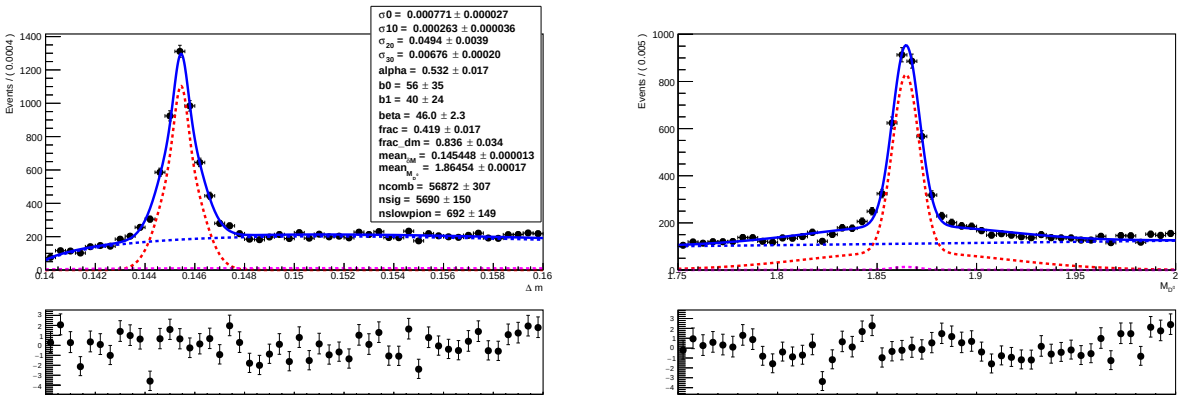

FIG. 24: ΔM (left) and M_D (right) 2D fit projections in DR2 sample for $D \to K\pi\pi\pi$ final state without PID.

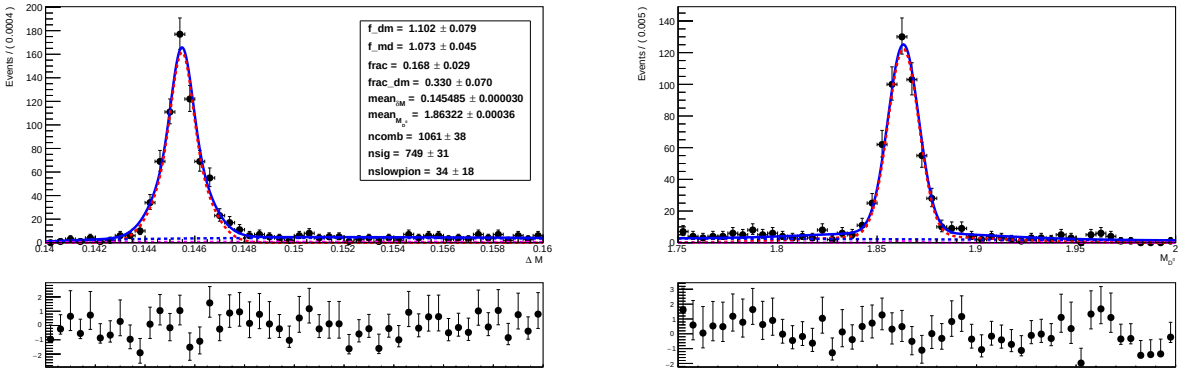

FIG. 25: ΔM (left) and M_D (right) 2D fit projections in 250 pb^{-1} prod4 data sample for $D \to K\pi$ final state without PID.

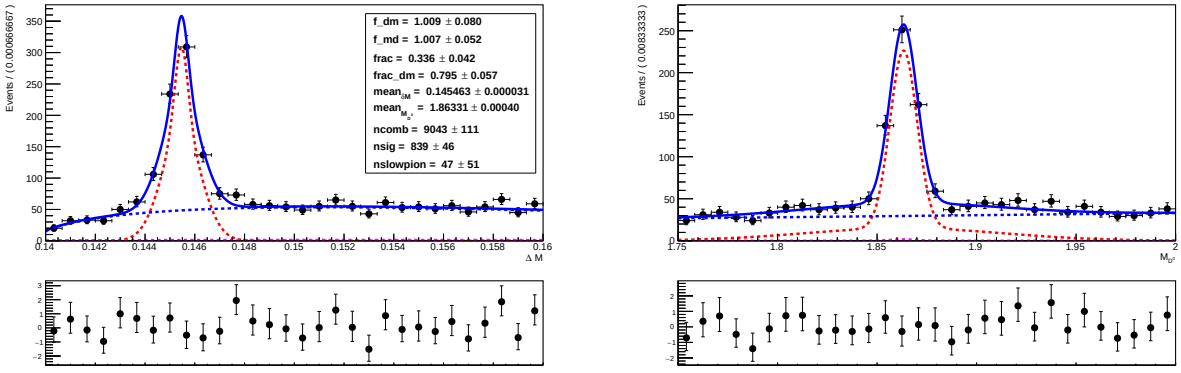

FIG. 26: ΔM (left) and M_D (right) 2D fit projections in 250 pb^{-1} prod4 data sample for $D \to K\pi\pi\pi$ final state without PID.

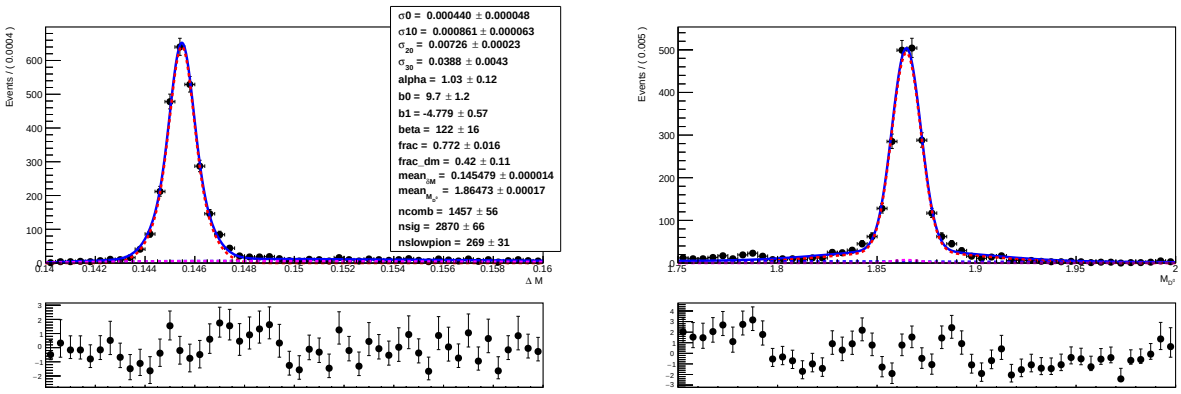

FIG. 27: ΔM (left) and M_D (right) 2D fit projections in DR2 sample for $D \to K\pi$ final state with PID.

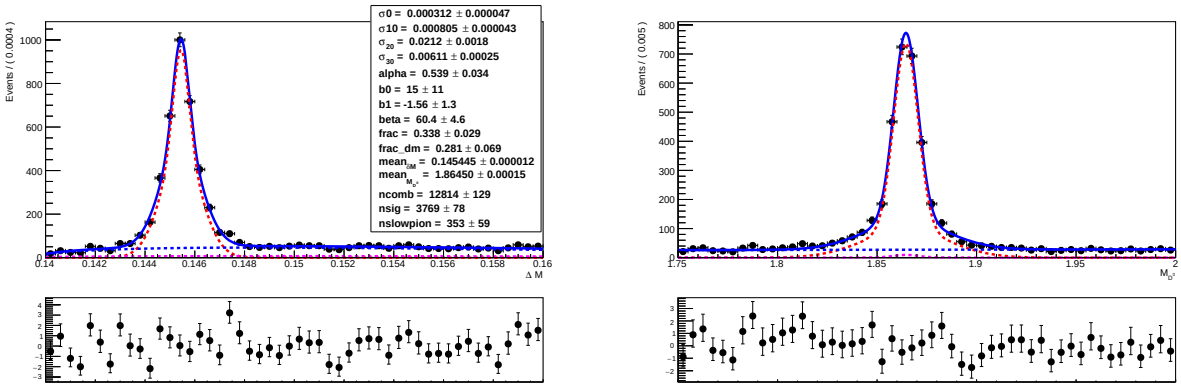

FIG. 28: ΔM (left) and M_D (right) 2D fit projections in DR2 sample for $D \to K\pi\pi\pi$ final state with PID.

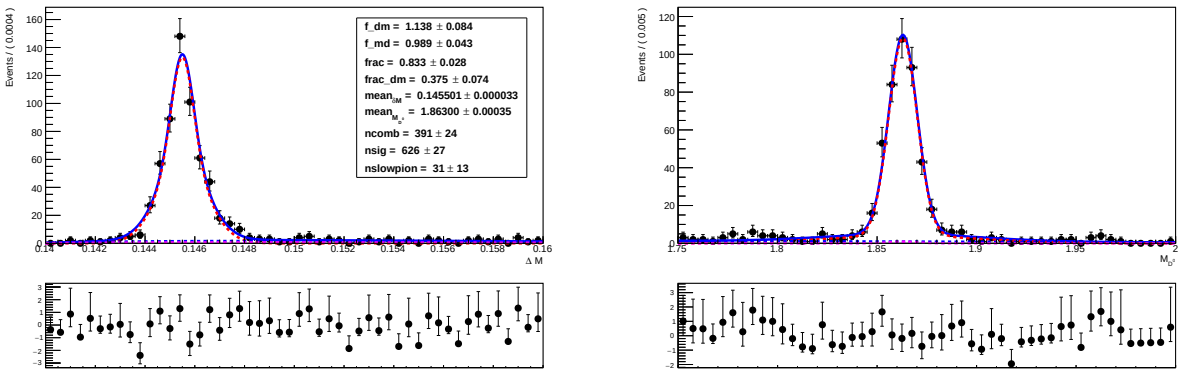

FIG. 29: ΔM (left) and M_D (right) 2D fit projections in 250 pb^{-1} prod4 data sample for $D \to K\pi$ final state with PID.

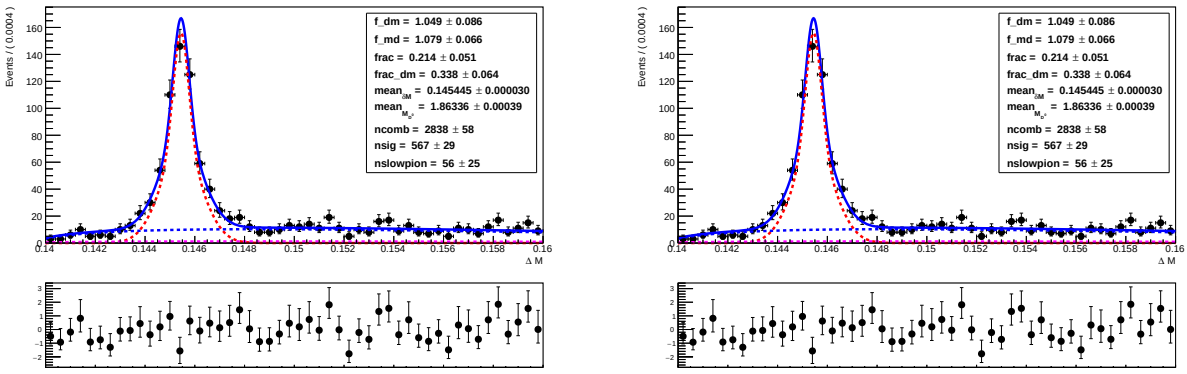

FIG. 30: ΔM (left) and M_D (right) 2D fit projections in 250 pb^{-1} prod4 data sample for $D \to K\pi\pi\pi$ final state with PID.

6. CP EIGENSTATES

6.1. $D \to K^+K^-$

$D \to K^+K^-$ is a CP even final state and also a singly Cabibbo suppressed mode. PID cut > 0.5 is applied on both the K. The M_D distribution before after applying PID are shown in Fig. 31.

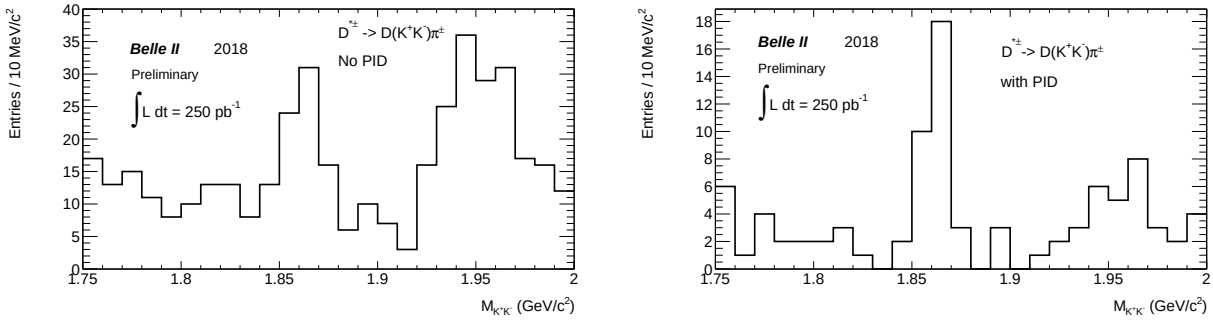

FIG. 31: M_D (right) distribution $D \to K^+K^-$ final state without (left) and with (right) PID cuts.

The mode is looked at in prod4 data sample and the ΔM and M_D distributions are shown in Fig. 33.

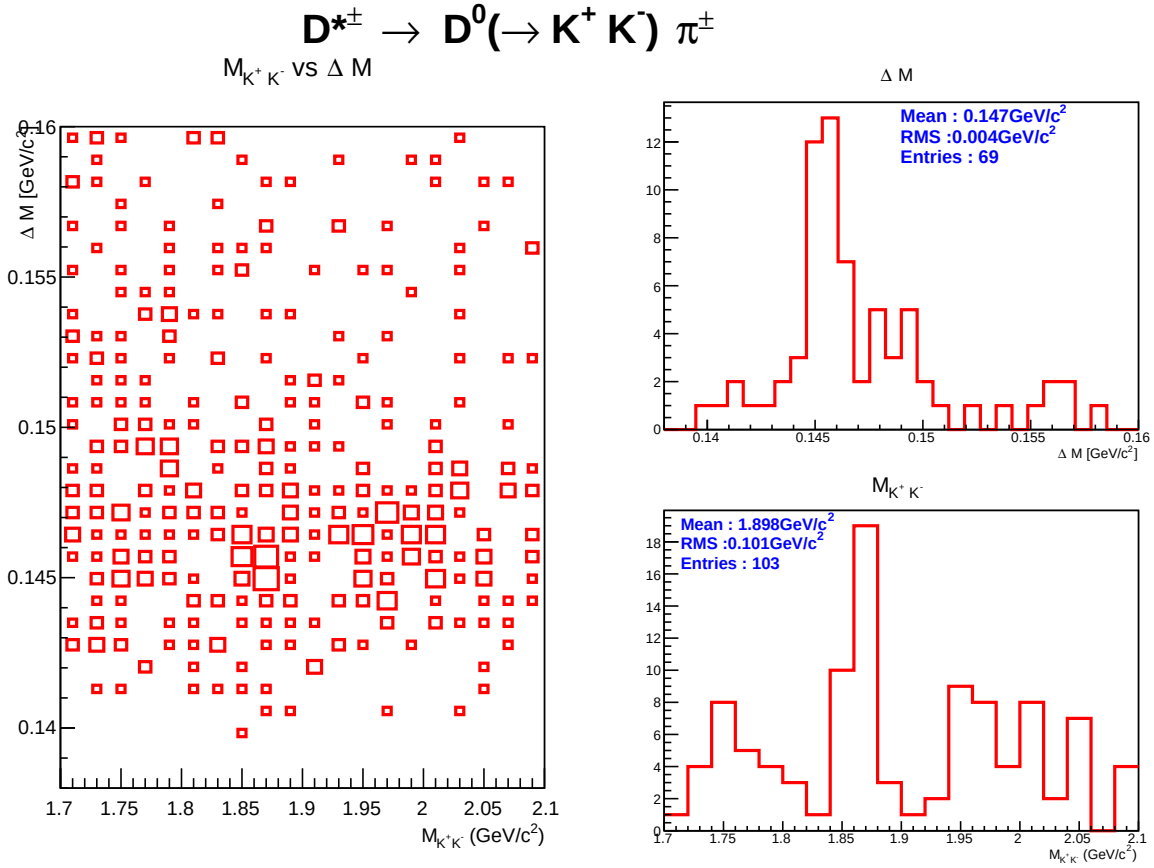

FIG. 32: 2D plot of ΔM and M_D (left), signal-enhanced plots: ΔM (right top) and M_D (right bottom) for $D \to K^+K^-$ final state in 250 pb^{-1} prod3 data.

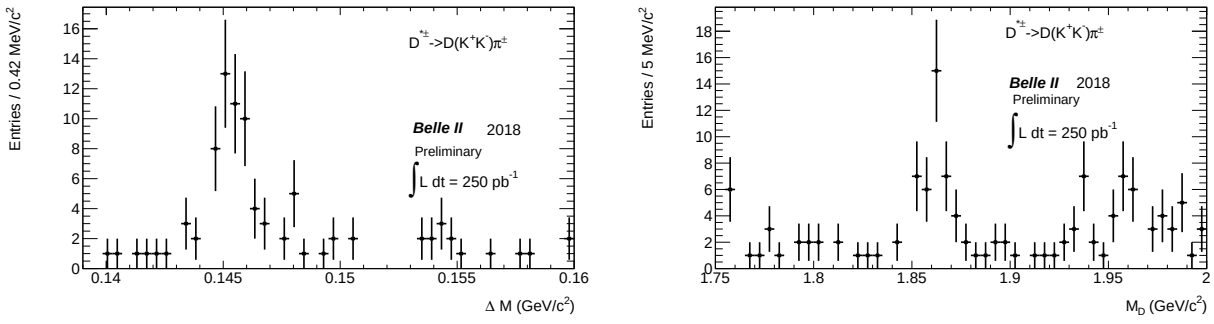

FIG. 33: ΔM (left) and M_D (right) signal-enhanced projections in 250 pb^{-1} prod4 data sample for $D \to K^+K^-$ final state.

6.2. $D \to K^0_S\pi^0$

$D \to K^0_S\pi^0$ is a CP odd final state and contains two neutral final states. We have used `standard`K_S list. The following cuts along with the other cuts mentioned above have applied for this mode.

- $0.45 < M(K_S) < 0.55$ GeV/c^2
- Signal region cuts:
  - $0.144 < \Delta M < 0.147$ GeV/c^2
  - $1.83 < M_D < 1.89$ GeV/c^2

Fig. 34 shows 2D plot of ΔM and M_D (left), signal-enhanced plots. A 2D fit has shown in Fig. 35.

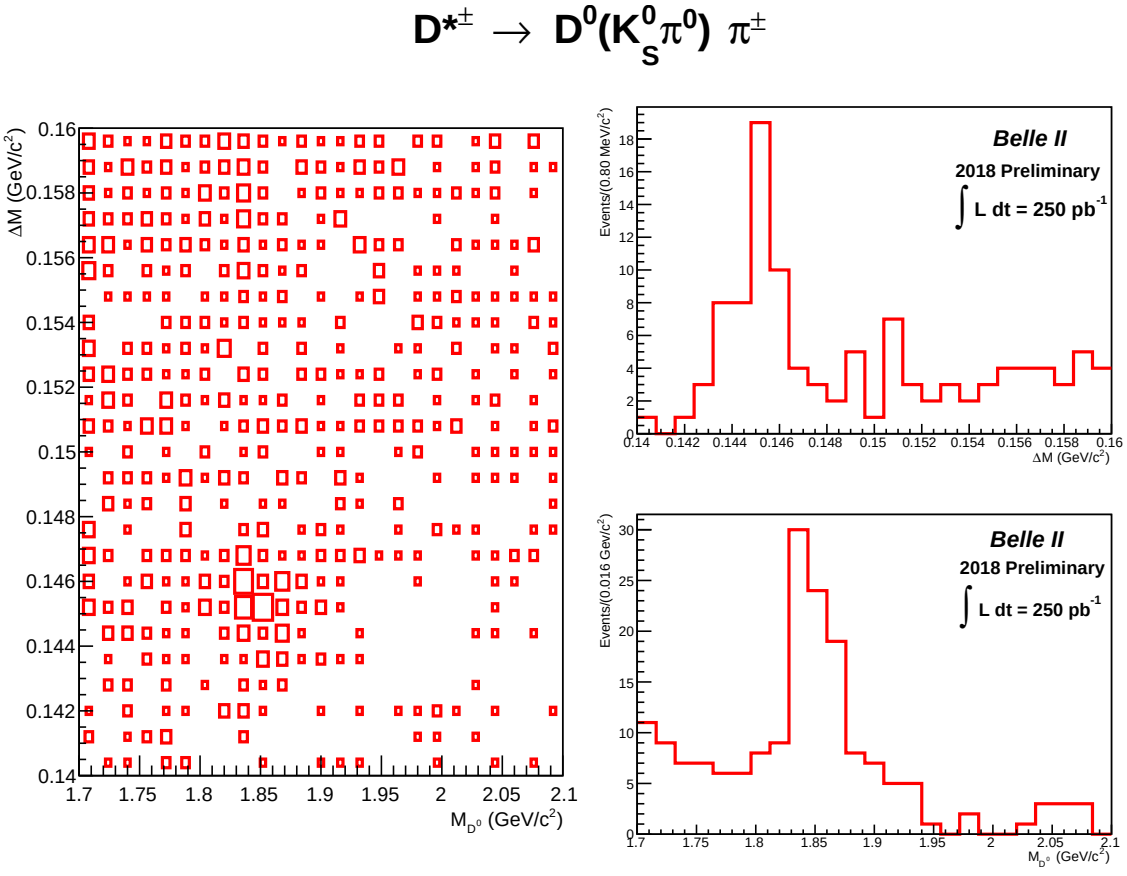

FIG. 34: 2D plot of ΔM and M_D (left), signal-enhanced plots: ΔM (right top) and M_D (right bottom) for $D \to K^0_S\pi^0$ final state in prod3 data.

The mode is looked at in prod4 data sample and the ΔM and M_D distributions are shown in Fig. 36. Here `mergedKs list` is used.

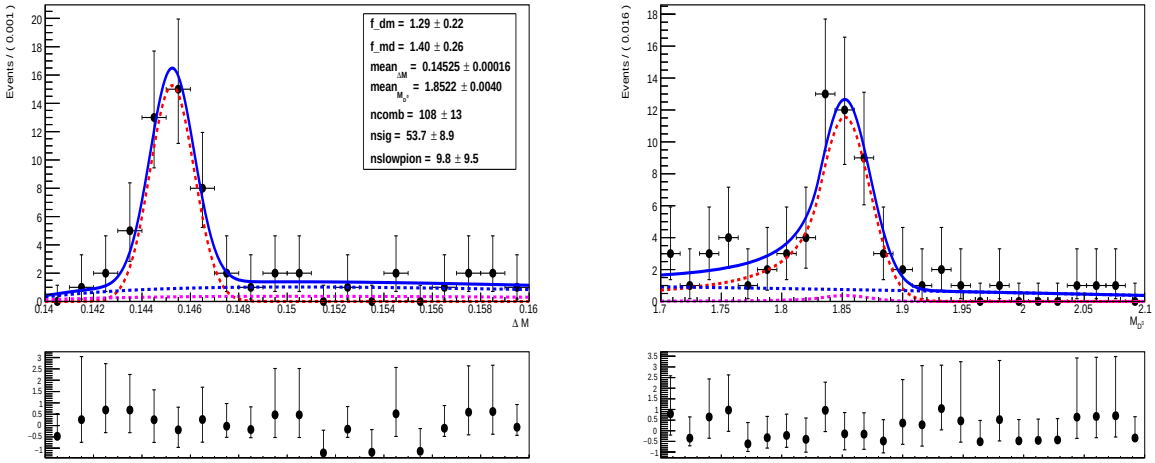

FIG. 35: ΔM (left) and M_D (right) signal-enhanced projections in 250 pb^{-1} prod3 data sample for $D \to K^0_S\pi^0$ final state.

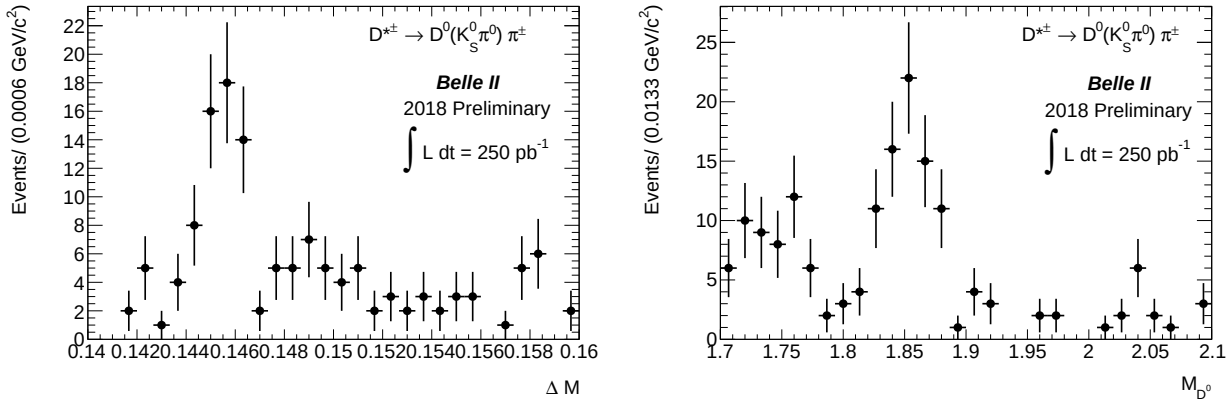

FIG. 36: ΔM (left) and M_D (right) signal-enhanced projections in 250 pb^{-1} prod4 data sample for $D \to K^0_S\pi^0$ final state.

Fig. 37 shows signal enhanced distributions of ΔM and M_D with `goodKs-selection`. A detailed description of `goodKs-selection` can be found in the BELLE2-NOTE-PH-2018-017.

The yields of various $D^{*\pm}$ modes are summarized in table IV. The yields are estimated from a two dimensional fit between M_D and ΔM except in the case of $K\pi\pi^0$. Due to high combinatorial background present, a one dimensional fit of ΔM is performed for $K\pi\pi^0$. PID > 0.5 is applied for K in all cases.

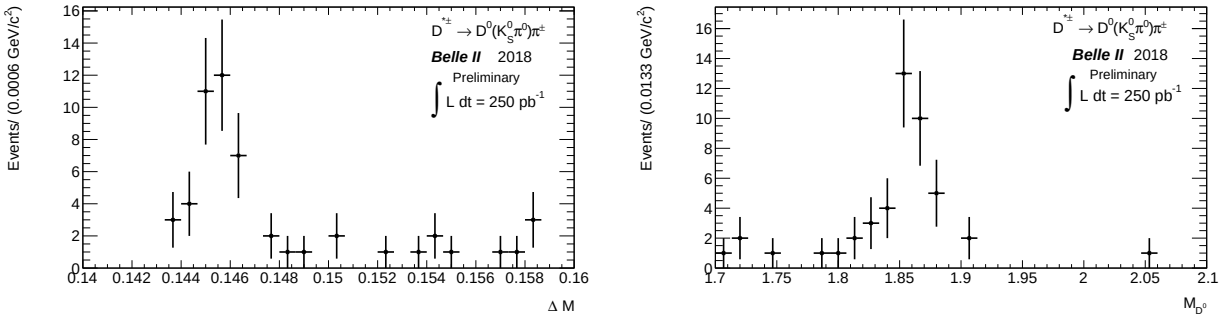

FIG. 37: ΔM (left) and M_D (right) signal-enhanced projections in 250 pb^{-1} prod4 data sample for $D \to K^0_S\pi^0$ final state.

Mode	yield	
	prod3	prod4
$D \to K^-\pi^+$	421 ± 22	565 ± 25
$D \to K^-\pi^+\pi^0$	969 ± 54	1012 ± 48
$D \to K^-\pi^+\pi^-\pi^+$	456 ± 25	524 ± 26
$D \to K^+K^-$	24 ± 6	41 ± 7
$D \to K^0_S\pi^0$	54 ± 9	39 ± 7
$D \to K^0_S\pi^+\pi^-$	28 ± 6	95 ± 11

TABLE IV: Yields of various $D^{*\pm}$ modes in 250 pb^{-1} prod3 and prod4 data sample. The yields are estimated from a two dimensional fit between M_D and ΔM except in the case of $K\pi\pi^0$. Due to high combinatorial background present, a one dimensional fit of ΔM is performed for $K\pi\pi^0$. PID > 0.5 is applied for K in all cases.

7. D^{*0} MODES

The D^{*0} mode is reconstructed from three different CF modes in prod3 data. These are the following. `looseFit`π^0 list is used.

- $D^{*0} \to D^0(K^-\pi^+)\pi^0$
- $D^{*0} \to D^0(K^-\pi^+\pi^0)\pi^0$
- $D^{*0} \to D^0(K^-\pi^+\pi^-\pi^+)\pi^0$

The following selections criteria are applied:

- $|d_0| < 0.5$ cm
- $|z_0| < 3$ cm
- $1.8 < M(K\pi) < 1.95$ GeV/c^2
- $0.134 < \Delta M < 0.15$ GeV/c^2
- $P^{D^*}_{cms} > 2.5$ GeV
- $PIDk > 0.6$

The signal region are selected as follows:

- For $K\pi$ and $K\pi\pi^0$ modes:
  - $0.1405 < \Delta M < 0.1425$ GeV/c^2
  - $1.855 < M_D < 1.875$ GeV/c^2
- For $K\pi\pi\pi$ modes:
  - $0.142 < \Delta M < 0.144$ GeV/c^2
  - $1.855 < M_D < 1.875$ GeV/c^2

The signal region cuts are little bit tighter than the cuts applied in $D^{(*\pm)}$ to reduce the background coming from π^0. The 2D plot of ΔM and M_D and signal enhanced plots are shown in Fig. 38, Fig. 39, Fig. 40. A 2D fit was performed for $DtoK\pi$ final states as shown is Fig. 41.

7.1. 250 pb^{-1} prod4 data

The CF final states of D^{*0} are analysed in the prod4 data sample and the ΔM and M_D distributions are shown in Fig. 42, 43, 44.

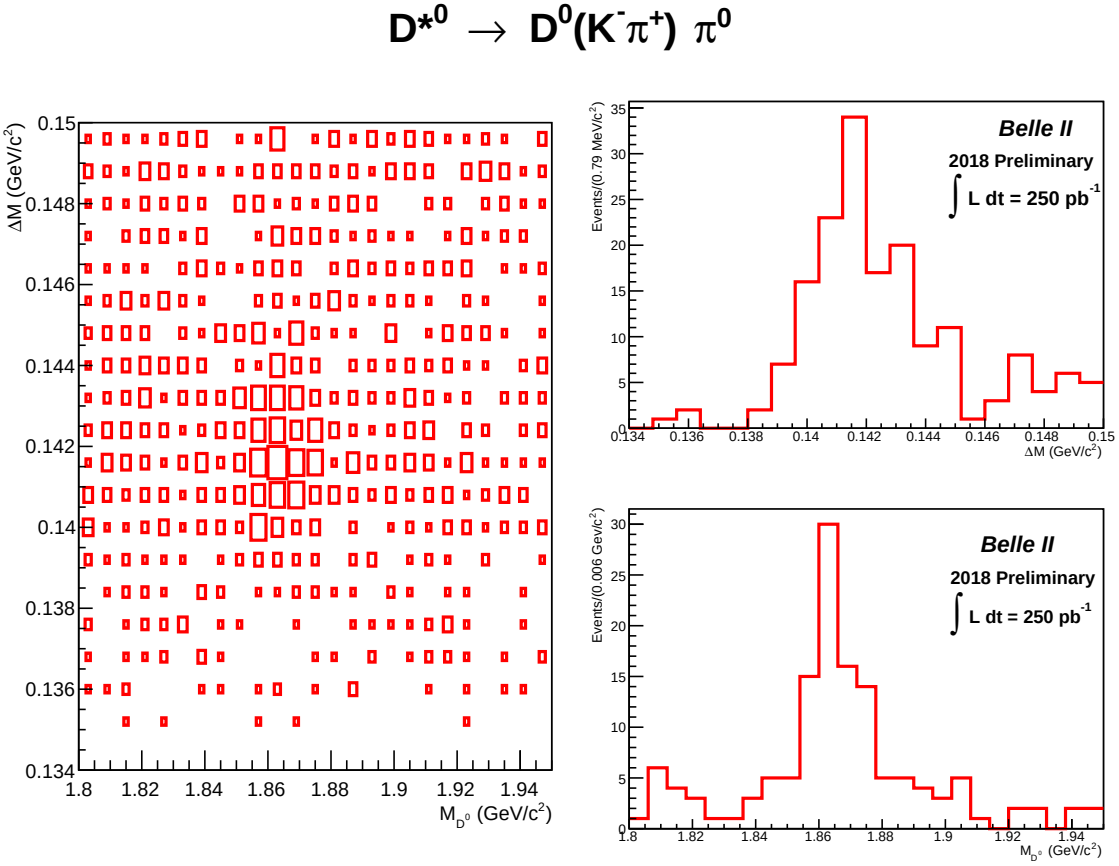

FIG. 38: 2D plot of ΔM and M_D (left), signal-enhanced plots: ΔM (right top) and M_D (right bottom) for $D^{*0} \to D^0(K^-\pi^+)\pi^0$ mode in prod3 data.

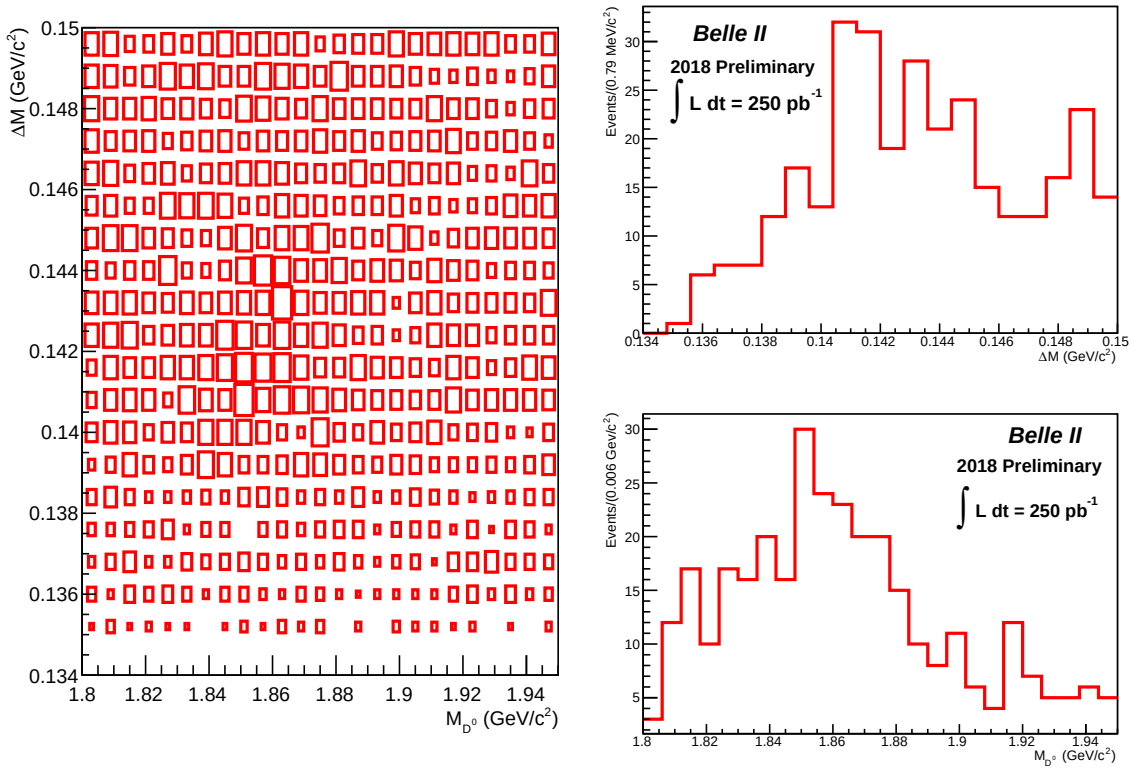

FIG. 39: 2D plot of ΔM and M_D (left), signal-enhanced plots: ΔM (right top) and M_D (right bottom) for $D^{*0} \to D^0(K^-\pi^+\pi^0)\pi^0$ mode in prod3 data.

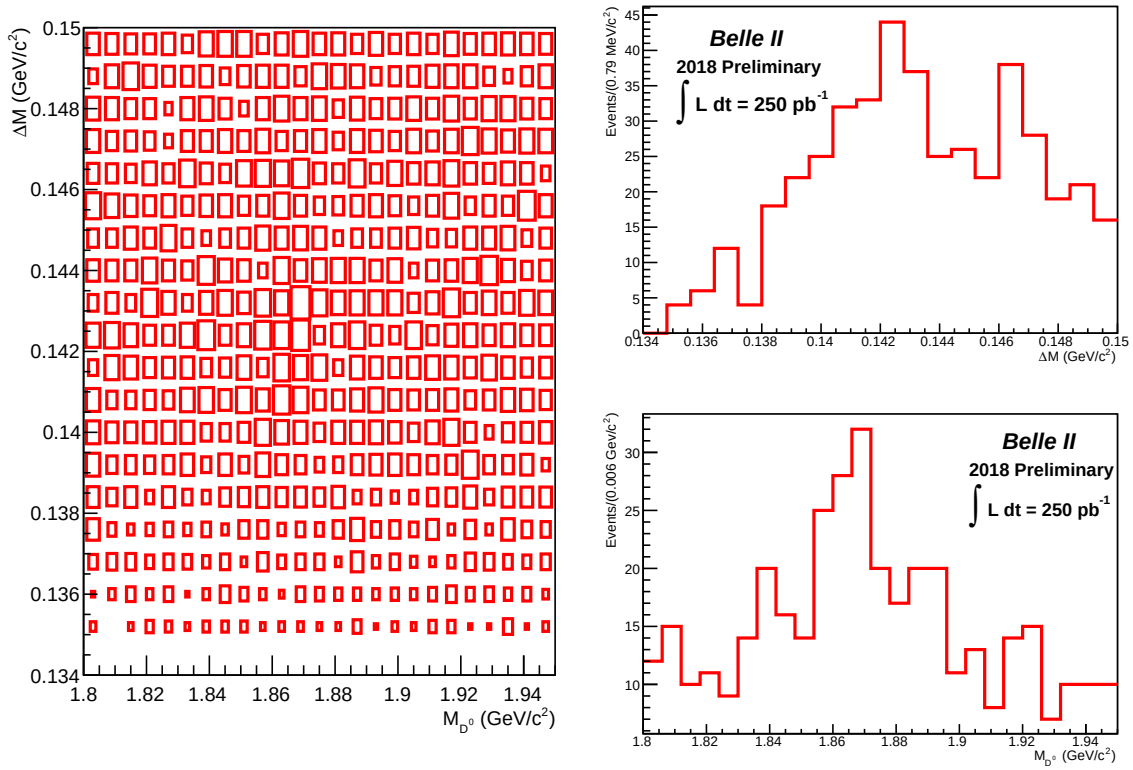

FIG. 40: 2D plot of ΔM and M_D (left), signal-enhanced plots: ΔM (right top) and M_D (right bottom) for $D^{*0} \to D^0(K^-\pi^+\pi^+\pi^-)\pi^0$ mode in prod3 data.

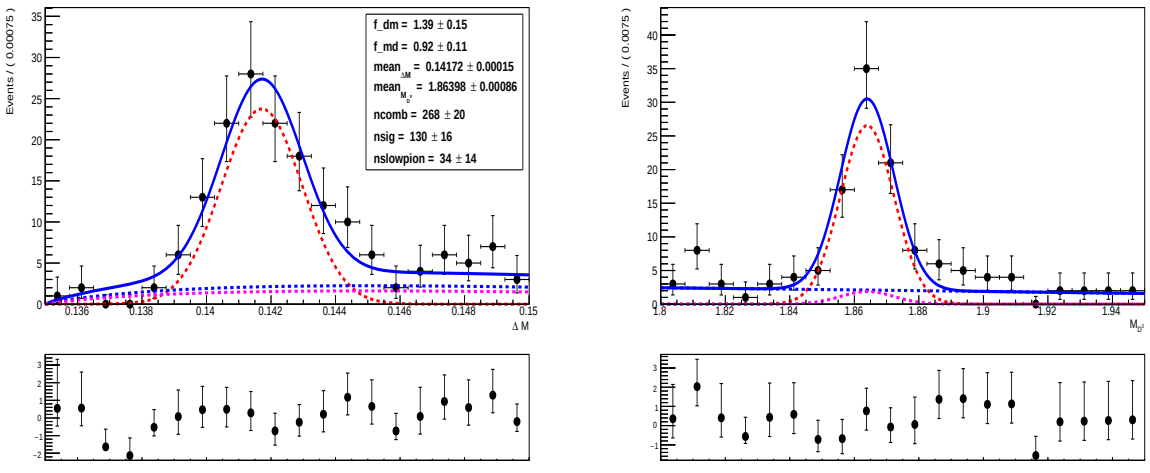

FIG. 41: ΔM (left) and M_D (right) signal-enhanced projections in 250 pb^{-1} prod3 data sample for $D^{*0} \to D^0(K^-\pi^+)\pi^0$ mode

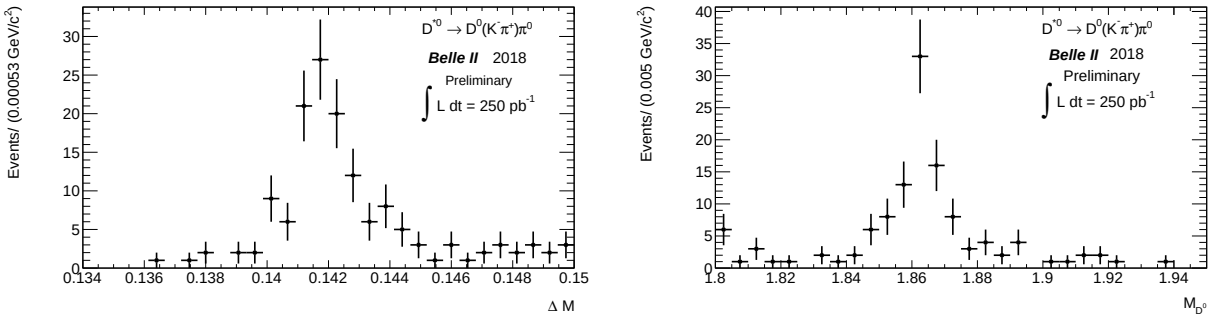

FIG. 42: ΔM (left) and M_D (right) signal-enhanced projections in 250 pb^{-1} prod4 data sample for $D \to K\pi$ final state.

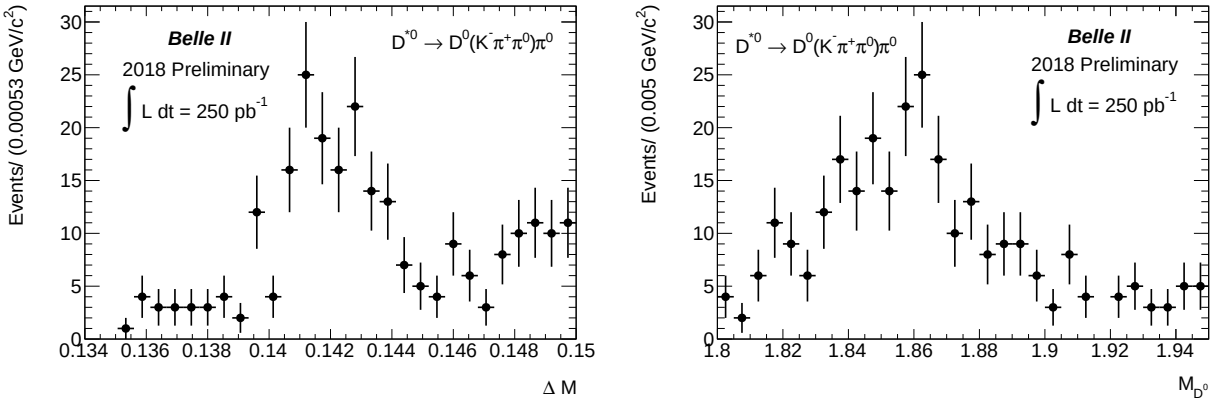

FIG. 43: ΔM (left) and M_D (right) signal-enhanced projections in 250 pb^{-1} prod4 data sample for $D \to K\pi\pi^0$ final state.

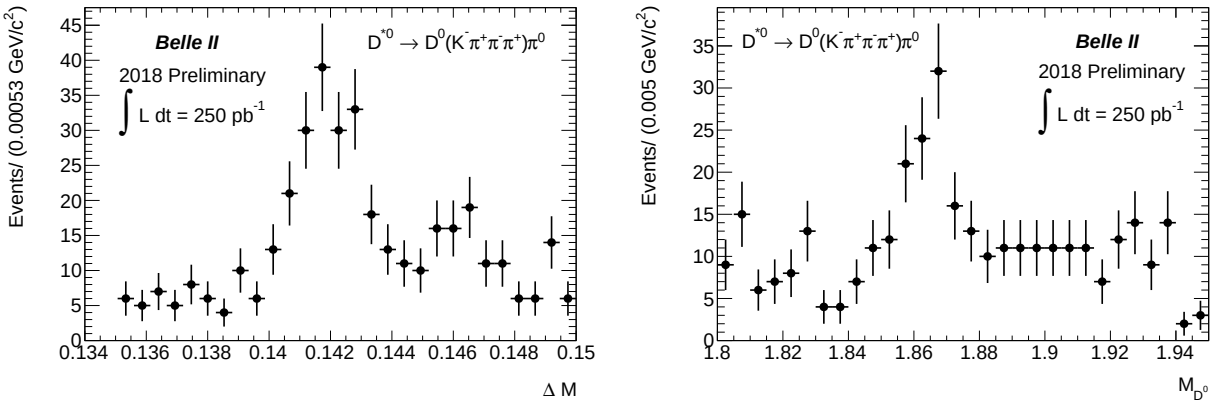

FIG. 44: ΔM (left) and M_D (right) signal-enhanced projections in 250 pb^{-1} prod4 data sample for $D \to K\pi\pi\pi$ final state.

8. $D^{\pm}$ MODES

The modes $D^{\pm} \to K^{\mp}\pi^{\pm}\pi^{\mp}$ and $D^{\pm} \to K^0_S\pi^{\pm}$ are analysed phase 2 data. The following selection criteria are applied.

- $|d_0| < 0.5$ cm
- $|z_0| < 3$ cm
- $1.7 < M_D < 2.1$ GeV/c^2
- $P^D_{cms} > 2$ GeV/c
- $0.47 < M_{K^0_S} < 0.53$ GeV/c^2

The samples are analysed first in DR2 sample and then in prod3 and prod4 samples. The M_D distributions in DR2 as well as prod3 data are shown in Fig. 45, 46. The M_D

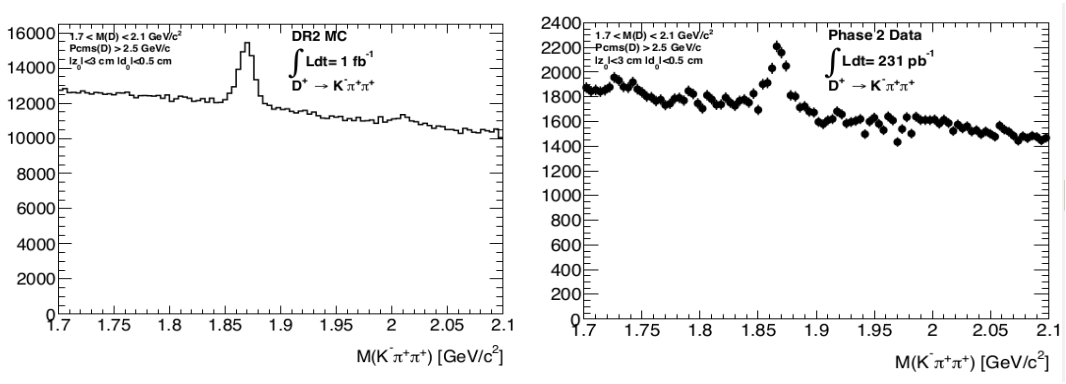

FIG. 45: M_D distribution in DR2 (left) and 250 pb^{-1} prod3 data sample for $D^{\pm} \to K^{\mp}\pi^{\pm}\pi^{\mp}$ mode

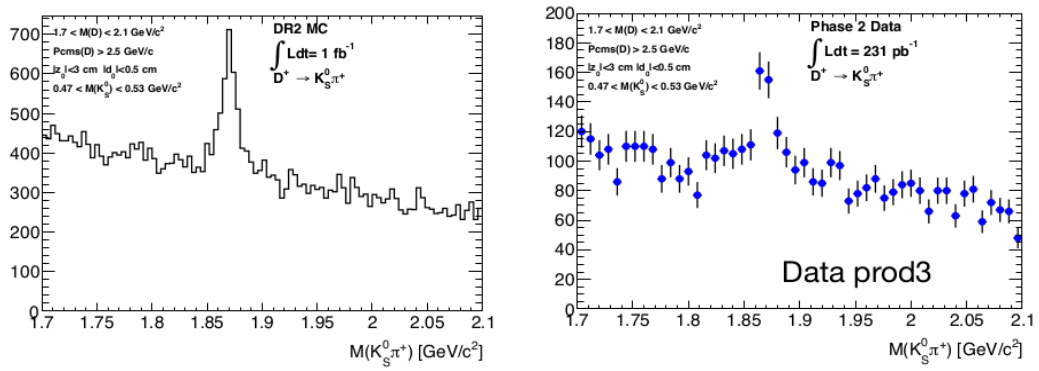

FIG. 46: M_D distribution in DR2 (left) and 250 pb^{-1} prod3 data sample for $D^{\pm} \to K^0_S\pi^{\pm}$ mode

distributions in prod4 data sample are shown in Fig. 47. For $D^{\pm} \to K^0_S\pi^{\pm}$, goodKs selection is applied as described in BELLE2-NOTE-PH-2018-017. This reduces more than 90% of the combinatorial bkg. This is illustrated in Fig. 48.

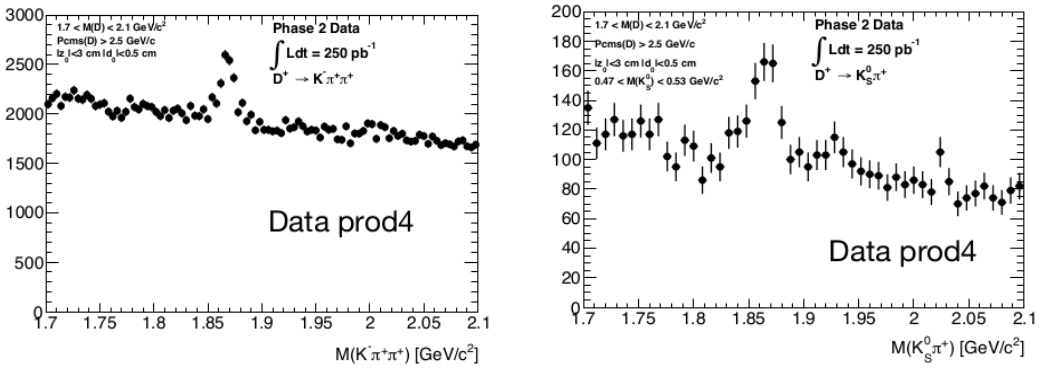

FIG. 47: M_D distribution in prod4 data sample for $D^{\pm} \to K^{\mp}\pi^{\pm}\pi^{\mp}$ (left) and $D^{\pm} \to K^0_S\pi^{\pm}$ (right) modes.

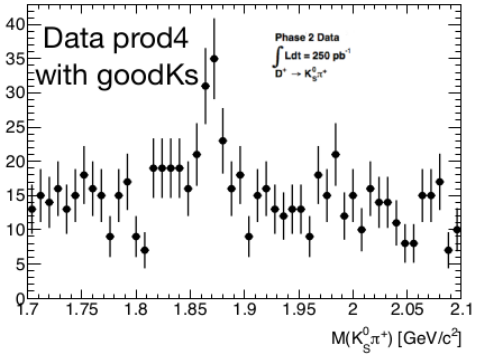

FIG. 48: M_D distribution in prod4 data sample for $D^{\pm} \to K^0_S\pi^{\pm}$ after goodKs selection.

9. REDISCOVERY OF B WITH $B \to D^{(*)}h$

The following selection criteria are used for different B modes.

- $|d_0| < 0.5$ cm
- $|z_0| < 3$ cm
- $0.489 < M_{K^0_S} < 0.506$ GeV/c^2.
- $1.84 < M_D < 1.89$ GeV/c^2
- $5.2 < M_{bc} < 5.29$ GeV/c^2
- $|\Delta E| < 0.2$ GeV
- KID > 0.5
- R2 < 0.3 for $B \to D\pi$, 0.25 for $B \to D\rho$, 0.4 for $B \to D^*\pi$ and $B \to D^*\rho$.
- $|M_\rho - m_{PDG}| < 100$ MeV/c^2.
- $0.140 < \Delta M < 0.144$ GeV/c^2 for D^{*0} and $0.143 < \Delta M < 0.147$ GeV/c^2 for $D^{*\pm}$.
- Signal region
  - $|\Delta E| < 0.05$ GeV
  - $M_{bc} > 5.27$ GeV/c^2

For $B \to D\pi$, all the three CF D final sates along with $K_S\pi^0$ and K^+K^- are used. The signal enhanced ΔE and M_{bc} distributions are shown in Fig. 49.

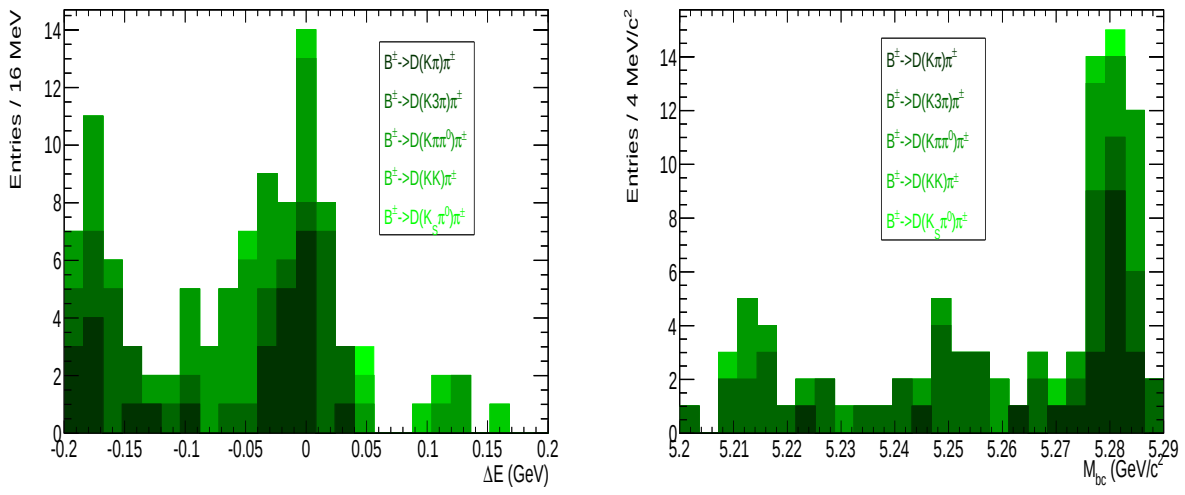

FIG. 49: ΔE (left) and M_{bc} (right) plots for $B^\pm \to D\pi^\pm$

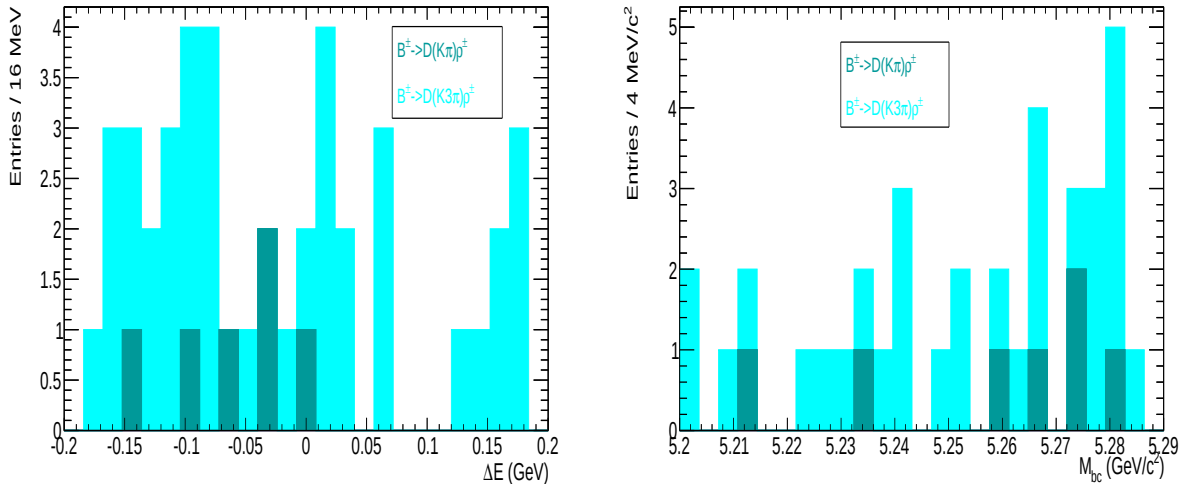

FIG. 50: ΔE (left) and M_{bc} (right) plots for $B^{\pm} \to D\rho^{\pm}$

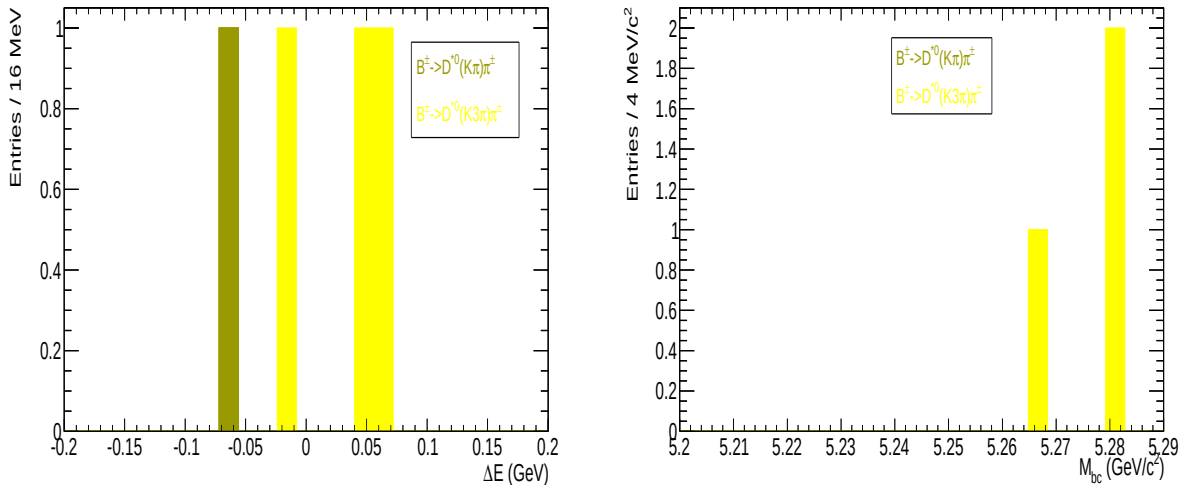

FIG. 51: ΔE (left) and M_{bc} (right) plots for $B^{\pm} \to D^{*0}\pi^{\pm}$

In $B^{\pm} \to D\rho^{\pm}$, the D final states used are $K\pi$ and $K\pi\pi\pi$. The plots are shown in Fig. 50. All the three CF final states for D are reconstructed for $B^{\pm} \to D^{*0}\pi^{\pm}$. The distribution is shown in Fig. 51. $B^0 \to D^{*\pm}\pi^{\mp}$ final state was also looked at with 3 CF modes as D final states. $B^0 \to D^{*\pm}\rho^{\mp}$ final state was analysed $K\pi$ and $K\pi\pi\pi$ as D final states and the plots are shown in Fig. 53. $B^0 \to D^{\pm}\pi^{\mp}$ modes are studied for $D^{\pm} \to K^{\mp}\pi^{\pm}\pi^{\mp}$ final state. The following selection criteria are used.

- $|d_0| < 0.5$ cm
- $|z_0| < 3$ cm
- $1.85 < M_D < 1.89$ GeV/c^2

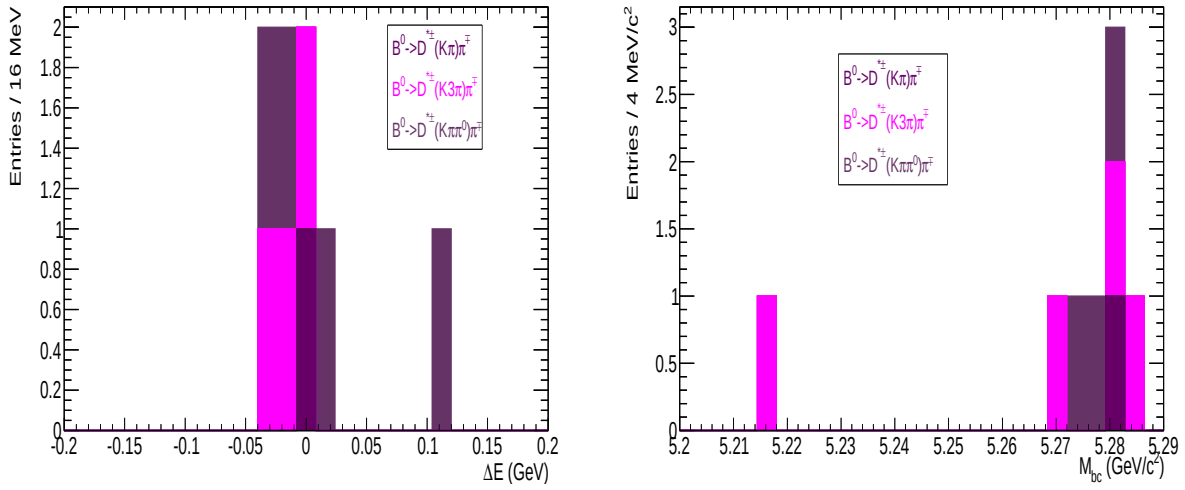

FIG. 52: ΔE (left) and M_{bc} (right) plots for $B^{\pm} \to D^{*\pm}\pi^{\mp}$

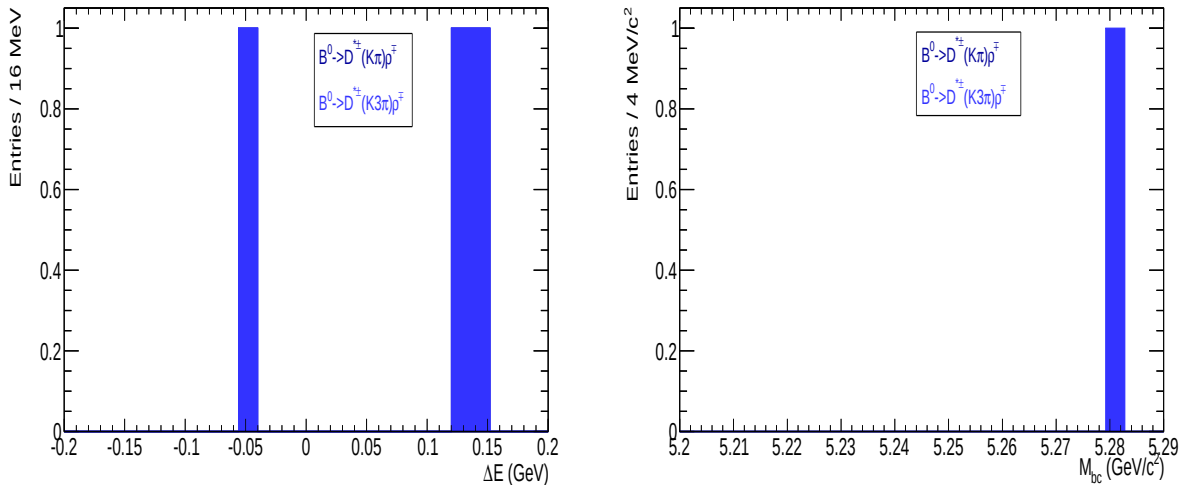

FIG. 53: ΔE (left) and M_{bc} (right) plots for $B^{\pm} \to D^{*\pm}\rho^{\mp}$

- $5.2 < M_{bc} < 5.29$ GeV/c^2
- $|\Delta E| < 0.1$ GeV
- R2 < 0.3

The ΔE and M_{bc} distributions in prod3 data sample are shown in Fig. 54. All the B final states including those described in BELLE2-NOTE-PH-2018-014 ($B \to J/\psi K^{(*)}$) are shown in Fig. 55. The yields from each of the modes by counting the number of events in signal region are given in table 9.

The distributions are studied in DR2 sample to model the signal and background shapes. A simultaneous fit is performed with final state without π^0 and with π^0. Signal component

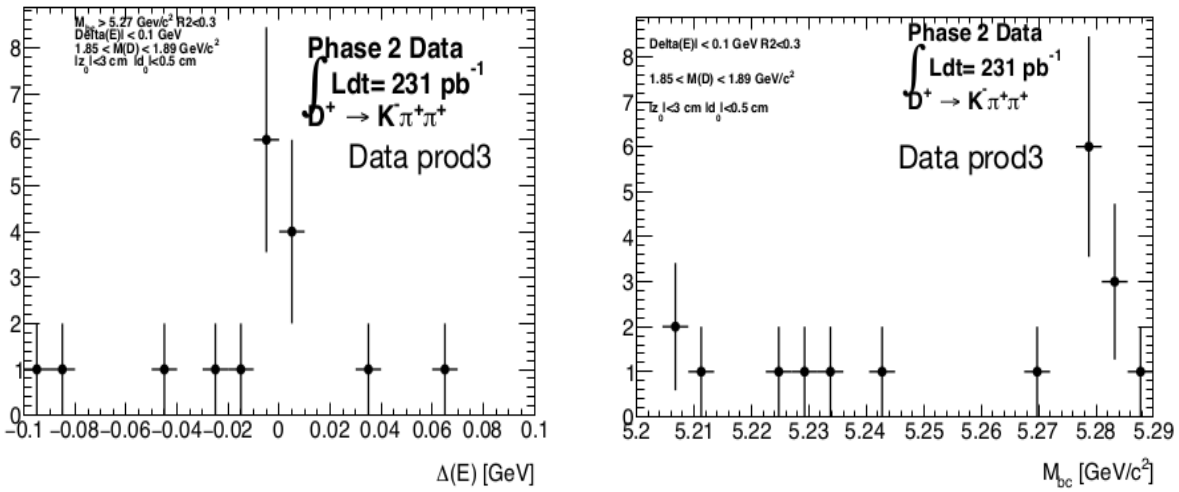

FIG. 54: ΔE (left) and M_{bc} (right) plots for $B^0 \to D^{\pm}\pi^{\mp}$

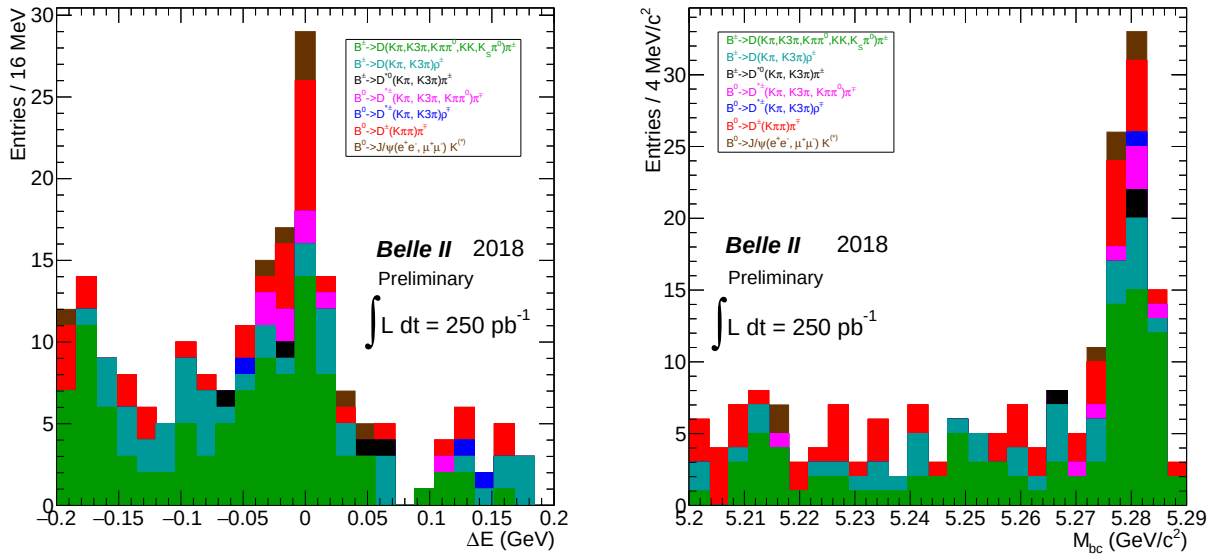

FIG. 55: ΔE (left) and M_{bc} (right) plots for $B \to D^{(*)}h$

in M_{bc} is described by a Gaussian and combinatorial with an Argus function. ΔE signal in category 1 is modelled with a Gaussian whereas in category 2 asymmetric Gaussian is used. ΔE combinatorial background is described by a landau function whose mean is fixed at -3. This is needed to account for the peaking structure appearing in lower ΔE region. Here $K\pi$, $K\pi\pi^0$ and $K\pi\pi\pi$ final states are reconstructed for D for $B^{\pm} \to D\pi^{pm}$ decay mode. The fit projections are shown in Fig. 56, 57.

The fit is done in data with all the modes specified above with fixing the shape parameters from DR2 fit. Modes with ρ are included in the second category. Mean, fudge factor and

Mode	yield
$B^{\pm} \to D\pi^{\pm}$	45
$B^{\pm} \to D\rho^{\pm}$	11
$B^{\pm} \to D^{*}\pi^{\pm}$	2
$B^{0} \to D^{*\pm}\pi^{\mp}$	7
$B^{0} \to D^{*\pm}\rho^{\mp}$	1
$B^{0} \to D^{\pm}\pi^{\mp}$	11
$B \to J/\psi K^{(*)}$	8

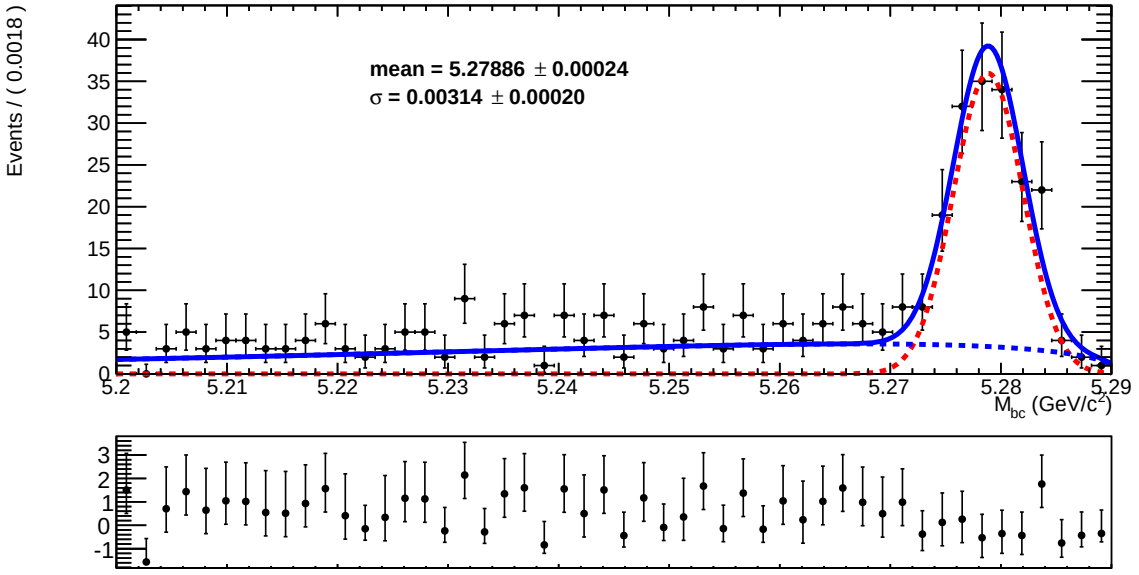

FIG. 56: M_{bc} fit projection in DR2 sample for $B^{\pm} \to D\pi^{\pm}$ with 3 CF D final states.

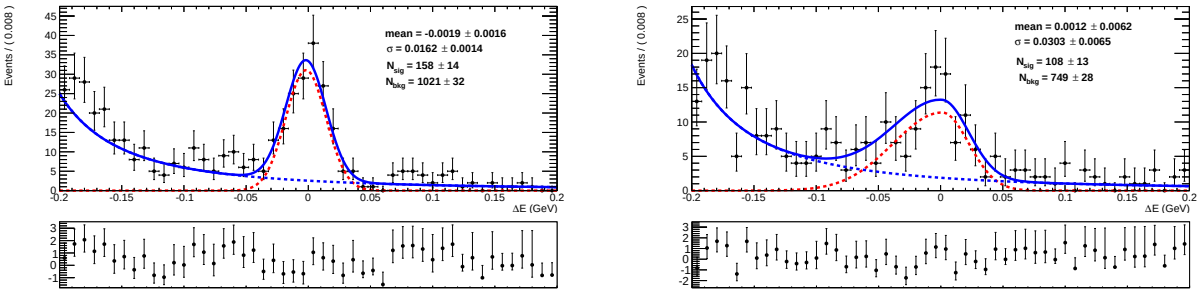

FIG. 57: ΔE fit projection in DR2 sample for $B^{\pm} \to D\pi^{\pm}$ with 3CF D final states with final state without π^0 (left) and final state with π^0 (right)

yields are floated. The fit projections are shown in Fig. 63, 64. There are 88 ± 8 signal B

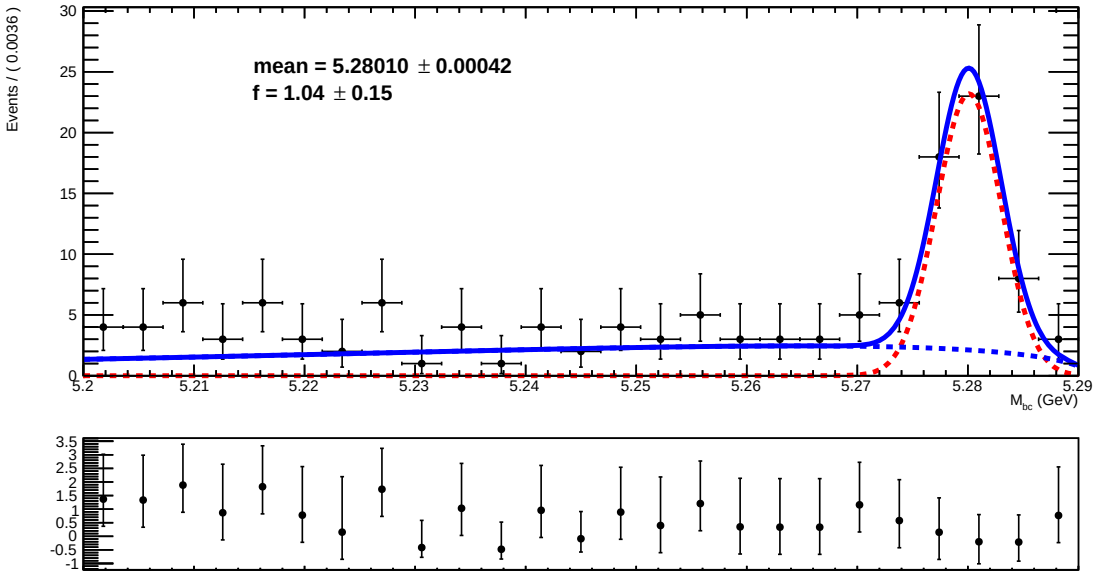

FIG. 58: M_{bc} fit projection in data for $B^{\pm} \to D\pi^{\pm}$ with 3 CF D final states.

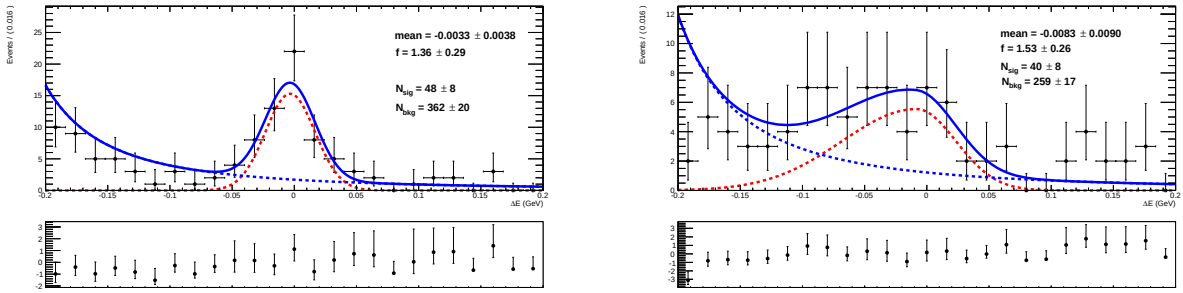

FIG. 59: ΔE fit projection in data for $B \to D^{(*)}h$ with final state without π^0 or ρ(left) and final state with π^0 and ρ (right)

candidates observed in total.

9.1. $B \to D^{(*)}h$ in prod4 sample

All the modes discussed in the previous section has been analysed with prod4 data sample. In addition $B^0 \to D^{\pm}\rho^{\mp}$ mode is also studied. The selection criteria are the same as for the other modes and ρ selection. PID > 0.5 applied on K. The distribution is shown in Fig. 60. The ΔE and M_{bc} distributions are shown in Fig. 61. The total ΔE and M_{bc} distributions with all the modes are shown in Fig. 62. The results from the simultaneous fit are shown in There are 96 ± 11 signal B candidates observed in total in prod4 data sample.

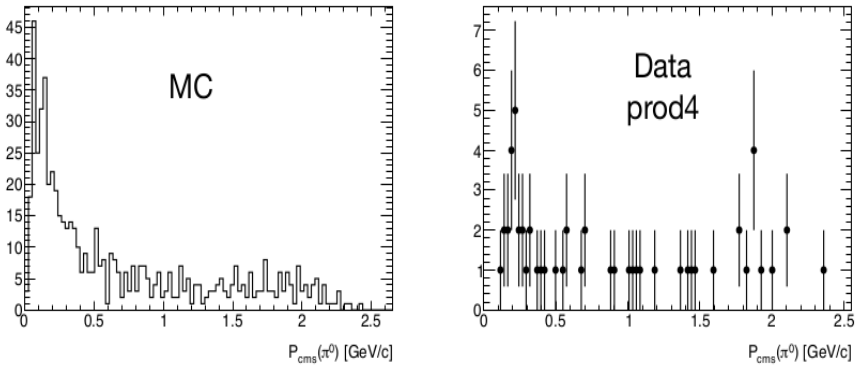

FIG. 60: p_{π^0} distribution in MC (left) and data (right) for $B \to D^{\pm}\rho^{\mp}$ mode.

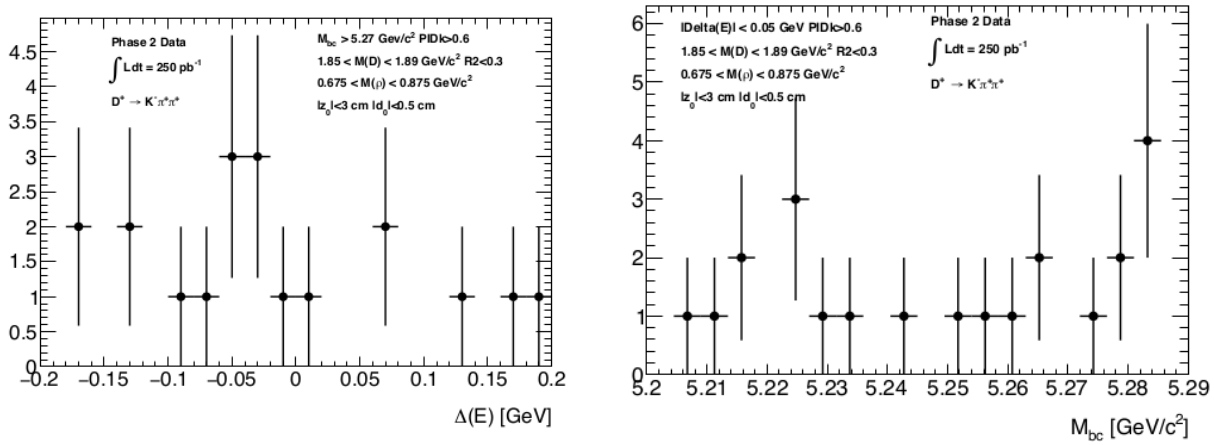

FIG. 61: ΔE (left) and M_{bc} (right) plots for $B \to D^{\pm}\rho^{\mp}$ mode in prod4 data

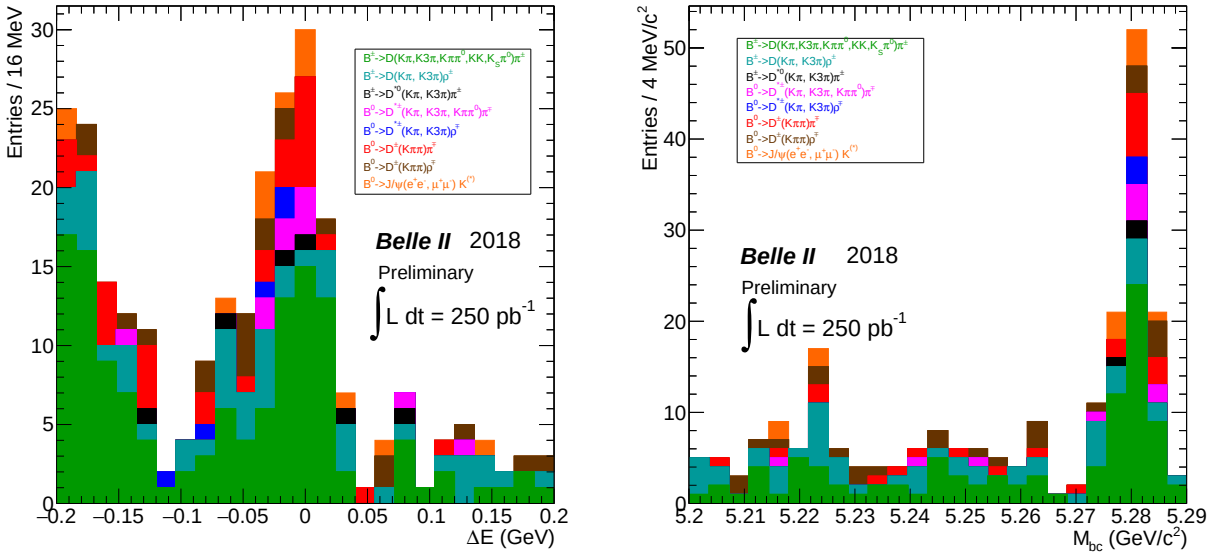

FIG. 62: ΔE (left) and M_{bc} (right) plots for $B \to D^{(*)}h$ and $B \to J/\psi K^{(*)}$ in prod4 data

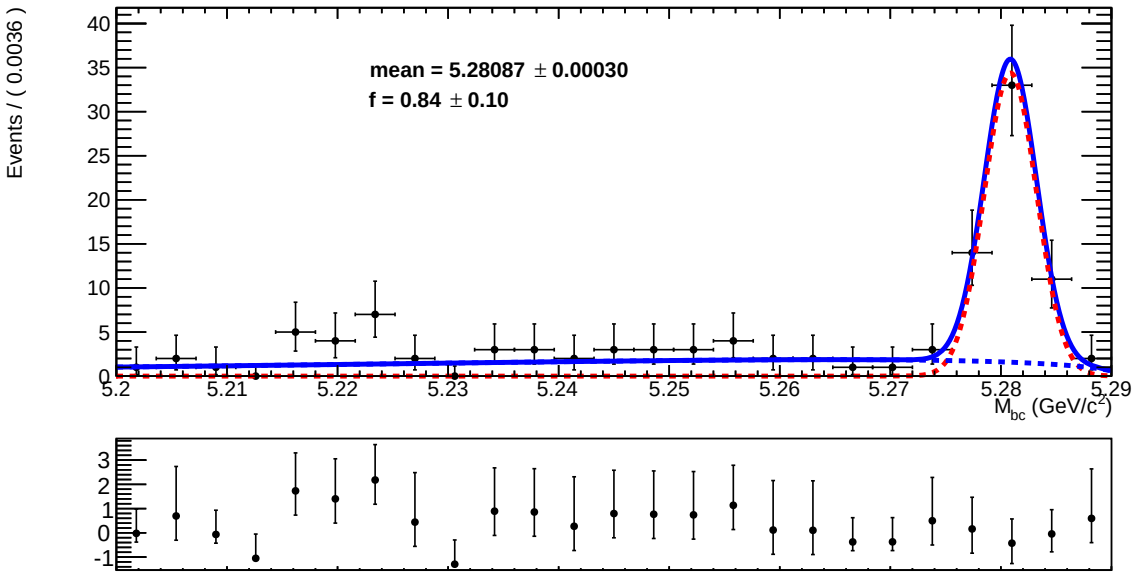

FIG. 63: M_{bc} fit projection in prod4 data.

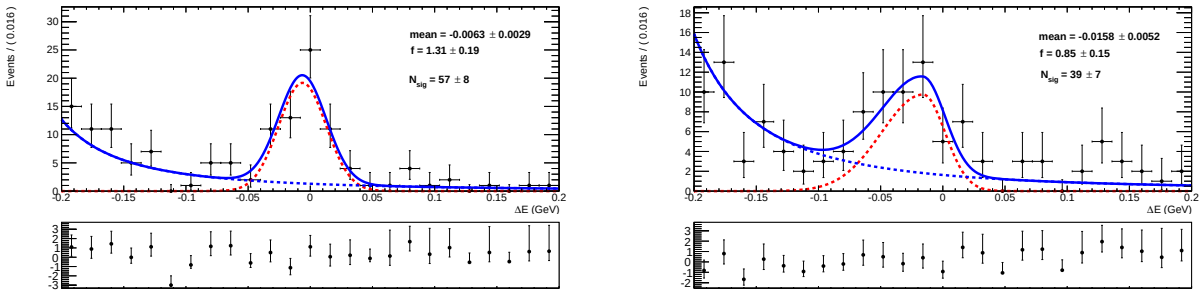

FIG. 64: ΔE fit projection in data for $B \to D^{(*)}h$ with final state without π^0 or ρ(left) and final state with π^0 and ρ (right)

9.2. Event Display

Fig. 65, 66 show the event display of a B event of the mode $B^{\pm} \to D(K^{-}\pi^{+})\pi^{\pm}$. The corresponding run number and event number are 3282 and 411102 respectively. The charged tracks are identified according to the momentum value.

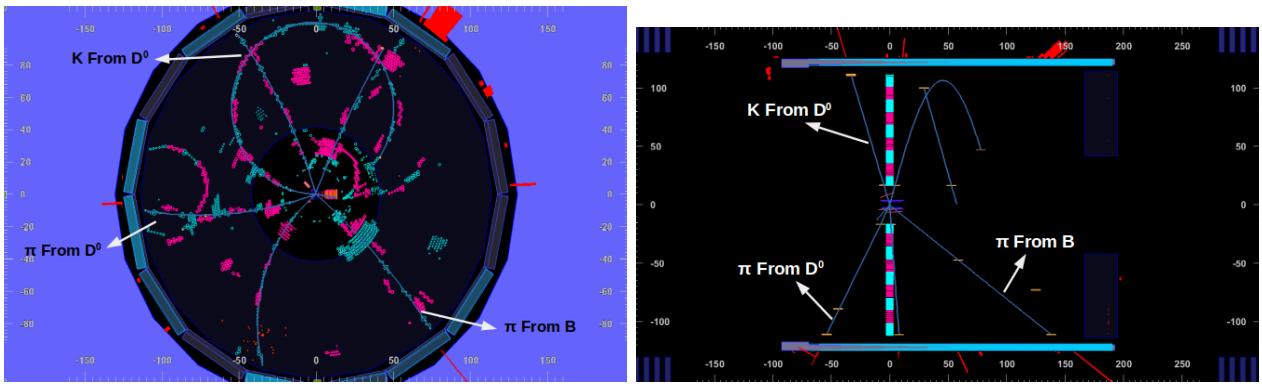

FIG. 65: $\rho - \phi$ (left) and $\rho - z$ (right) view

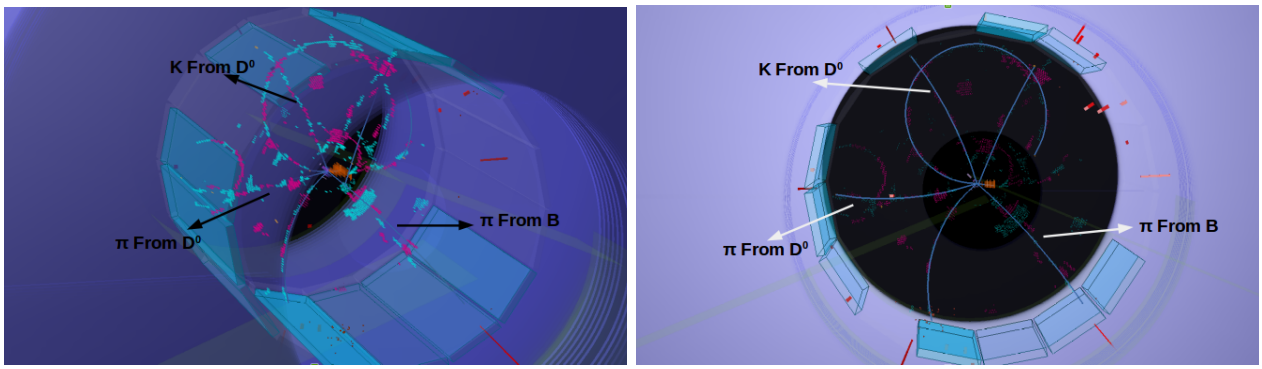

FIG. 66: 3D view